From the Department of Molecular Medicine and Surgery
Karolinska Institutet, Stockholm, Sweden

Cardiovascular Magnetic Resonance Evaluation of Effusive and Constrictive Physiologies

Simon Olof Anders Thalén

Stockholm 2024

All previously published papers were reproduced with permission from the publisher.
Published by Karolinska Institutet.
Printed by Universitetsservice US-AB, 2024
© Simon Thalén, 2024
ISBN 978-91-8017-279-0
Cover illustration: A drawing illustrating the intertwined concepts from mathematics, physics and medicine that form cardiovascular magnetic resonance. Courtesy of Signe Thalén.
All un-attributed illustrations were made by the author

Cardiovascular Magnetic Resonance Evaluation of Effusive and Constrictive Physiologies

Thesis for Doctoral Degree (Ph.D.)

By

Simon Olof Anders Thalén

The thesis will be defended in public at Nya Karolinska Solna, Clarence Crafoord lecture hall, NKS/U1/A504 at 09:00 on February 22 2024

Principal Supervisor:
Martin Ugander
Karolinska Institutet
Department of Molecular Medicine and Surgery
Unit of Clinical Physiology

Co-supervisors:
Andreas Sigfridsson
Karolinska Institutet
Department of Molecular Medicine and Surgery
Unit of Clinical Physiology

Peder Sörensson
Karolinska Institutet
Department of Medicine
Unit of Cardiology

Opponent:
Subha Rahman
Indiana University School of Medicine
Division of Cardiology

Examination Board:
Eric Rullman
Karolinska Institutet
Department of Laboratory Medicine
Unit of Clinical Physiology

Torkel Brismar
Karolinska Institutet
Department of Clinical Science, Intervention and Technology
Unit of Radiology

Elmir Omerovic
Sahlgrenska University Hospital
Department of Cardiology

Dedicated to Saijai and Signe

Abstract

This thesis presents an exploration of cardiovascular magnetic resonance (CMR) in the evaluation of effusive and constrictive heart conditions. Central to the thesis is advanced CMR as a diagnostic tool in pericardial effusion and constrictive pericarditis.

Studies I and II concern the application of T1 mapping for the characterization of pleural and pericardial effusions and attempts to enhance the understanding of the dynamics of extracellular gadolinium-based contrast agents (GBCA) in effusion fluid.

Study II establishes normal T1 values at 1.5 T in the pericardial fluid of healthy individuals, providing a benchmark for future studies.

Studies III and IV concern ventricular interdependence, a crucial aspect in evaluating constrictive physiology. Ventricular interdependence is measured by quantifying the respiratory variation in peak early transvalvular blood flow velocities. In **Study III**, an open-source software tool to perform semi-automated image analysis of real-time phase contrast (RT-PC) images is developed, and normal values are established. In **Study IV,** the repeatability and reproducibility of the method are tested.

This thesis concludes that CMR can become a valuable tool in evaluating pericardial effusion and constrictive pericarditis. Both molecular imaging evaluation of effusive fluids and hemodynamic assessment of ventricular interdependence are feasible using CMR.

Popular science summary of the thesis

This thesis concerns two ways to use magnetic resonance imaging (MRI) to gather information about a patient's inner workings so that their doctor can use it to help decide how to treat them best. MRI is great because it is harmless and involves no radiation. The thesis concerns two main categories of patients. Patients with too much fluid around their heart and patients where the surface of the heart has become rigid and stiff. In both these categories of patients, the heart is being squeezed from the outside, like being stuck in a vice. The first technique is T1 mapping, and the thesis explores if it can say something useful about the fluid around the heart. Knowing what the fluid is can help determine where it comes from and how it should be dealt with. The second is a real-time phase contrast technique that measures how fast the blood flows and fills the heart. In both these two categories of patients, squeezing the heart causes the filling of the heart to work in a peculiar way as the patient breathes. This thesis offers a simple and easy-to-use method for MRI to see that. For various reasons, this thesis did not manage to prove that these two techniques can be used effectively in these two categories of patients. However, valuable insights are still presented. This is often the case in science, where mountains are climbed together, one step at a time, one person after another. The knowledge gained by the strenuous efforts in this thesis will provide a stepping stone for someone else.

List of scientific studies included in the thesis

I. **Thalén S**, Maanja M, Sigfridsson A, Maret E, Sörensson P, Ugander M. The dynamics of extracellular gadolinium-based contrast agent excretion into pleural and pericardial effusions quantified by T1 mapping cardiovascular magnetic resonance. J Cardiovasc Magn Reson. 2019 14;21(1):71.

II. **Thalén S**, Ramos JG, Engblom H, Sigfridsson A, Sörensson P, Ugander M. Normal values for native T1 at 1.5 T in the pericardial fluid of healthy volunteers. European Heart Journal - Imaging Methods and Practice. 2023 Sep 1;1(2):qyad028

III. **Thalén S**, Heiberg E, Sörensson P , Giese D, Sigfridsson A, Ugander M. Normal values for mitral and tricuspid early inflow blood flow velocity variation using real time phase contrast cardiovascular magnetic resonance. *Submitted*

IV. **Thalén S**, Wieslander B, Sigfridsson S, Giese D, Sörensson P, Ugander M. Test-retest repeatability and inter-observer reproducibility of ventricular interdependence measured using semi-automatic analysis of real time phase contrast cardiovascular imaging. *Manuscript*

List of studies not included in the thesis

Thalén S, Lundberg G, Razuvaev A. *A single bilateral renal artery embolus traversing the aortic lumen – a hammock embolus*. Annals of Vascular Surgery - Brief Reports and Innovations. 2023 Mar;3(1):100158.

Ramos JG, Fyrdahl A, Wieslander B, **Thalén S**, Reiter G, Reiter U, et al. Comprehensive Cardiovascular Magnetic Resonance Diastolic Dysfunction Grading Shows Very Good Agreement Compared With Echocardiography. JACC Cardiovasc Imaging. 2020 Dec;13(12):2530–42.

Nickander J, Themudo R, **Thalén S**, Sigfridsson A, Xue H, Kellman P, et al. The relative contributions of myocardial perfusion, blood volume and extracellular volume to native T1 and native T2 at rest and during adenosine stress in normal physiology. J Cardiovasc Magn Reson. 2019 Dec;21(1):73.

Thalén S, Forsling I, Eintrei J, Söderblom L, Antovic JP. Pneumatic tube transport affects platelet function measured by multiplate electrode aggregometry. Thromb Res. 2013 Jul;132(1):77–80.

Contents

1 Introduction 1
1.1 Pericardial effusion 1
1.1.1 Pleural effusion 1
1.1.2 Pathophysiology and Starling forces 2
1.1.3 Epidemiology 3
1.1.4 Transudates and Exudates 4
1.1.5 Treatment 6
1.2 Constrictive pericarditis 6
1.2.1 Pathophysiology 6
1.2.2 Epidemiology and Diagnosis 6
1.2.3 Treatment 7
1.3 Ventricular Interdependence 7
1.4 Magnetic Resonance Imaging 9
1.4.1 Basic Imaging Physics 9
1.4.2 Faraday Induction 10
1.4.3 The Concept of Resonance 12
1.4.4 Achieving Rotation in the M_{xy} Plane 12
1.4.5 T1 relaxation, T2 decay and Free Induction Decay 13
1.4.6 Significance of Fourier analysis 14
1.4.7 Significance and Proof of Euler's Formula 15
1.4.8 Slice Selection, Phase and Frequency Encoding 16
1.4.9 T1 mapping 18
1.4.10 Excretion of contrast agents 19
1.4.11 Phase Contrast Velocity Encoded Imaging 20
1.4.12 Eddy Currents 21
1.5 Repeatability, Reproducibility, Agreement and Bias 22
2 Aims 25
3 Materials and Methods 27
3.1 Study Populations 27
3.2 Ethical Considerations 29
3.3 Cardiovascular Magnetic Resonance Imaging 30
3.4 T1 Mapping 30
3.5 T1 mapping Image Analysis 32
3.6 Real-Time Phase-Contrast Velocity Encoded Imaging 34
3.7 Semi-Automatic Analysis of RT-PC Images 35

3.8 Statistical Analysis 36
4 Results 37
4.1 T1 Mapping and Contrast Dynamics 37
4.2 Ventricular Interdependence 43
5 Discussion 47
5.1 Native T1 and GBCA Contrast Dynamics 47
5.2 The Light Criteria 49
5.3 Real-Time Phase Contrast Imaging 51
5.4 Arithmetic Considerations to Respiratory Variation 52
5.5 Methodological Considerations In Respiratory Variation 53
5.6 Repeatability and reproducibility 54
6 Conclusions 57
7 Points of perspective 59
8 Catharsis 60
8.1 Underestimating the Time Required and Difficulty of a Task 60
8.2 Failure to Collaborate 61
8.3 You Cannot Pop a Burned Popcorn 62
8.4 Sometimes Grit is not Enough 62
9 Acknowledgments 62
10 References 64

List of abbreviations

MRI	Magnetic resonance imaging
CMR	Cardivascular magnetic resonance
RT-PC	Real-time phase contrast
GBCA	Gadolinium based contrast agent
CT	Computerized tomography
VENC	Velocity encoding gradient
bSSFP	Balanced steady state free precession
IHD	Ischemic heart disease
LV	Left ventricle
EF	Ejection fraction
LVEF	Left ventricular ejection fraction
LVH	Left ventricular hypertrophy
DCM	Dilated cardiomyopathy
FOV	Field of view
Vinsp	Inspiratory transvalvular peak early velocity
Vexp	Expiratory transvalvular peak early velocity
ICC	Intraclass correlation coefficient
MOLLI	Modified Look-Locker imaging
RF	Radio frequency
ECV	Extracellular volume

1 Introduction

1.1 Pericardial effusion

The pericardium is comprised of two layers of connective tissue enveloping the heart. Its physiological function is to protect and hold the heart in the mediastinum, constrain chamber dilation, and optimize the pressure and volume relationship within the heart (1). The space between the inner and outer layers typically contains between 15 and 50 mL of pericardial fluid acting as a lubricant facilitating the independent movement of the surfaces of the inner and outer layers (2). An abnormal excess of fluid is referred to as a pericardial effusion. The clinical severity of a pericardial effusion can range from asymptomatic to life-threatening (3). A healthy heart and a heart with pericardial effusion is shown in **Figure 1**.

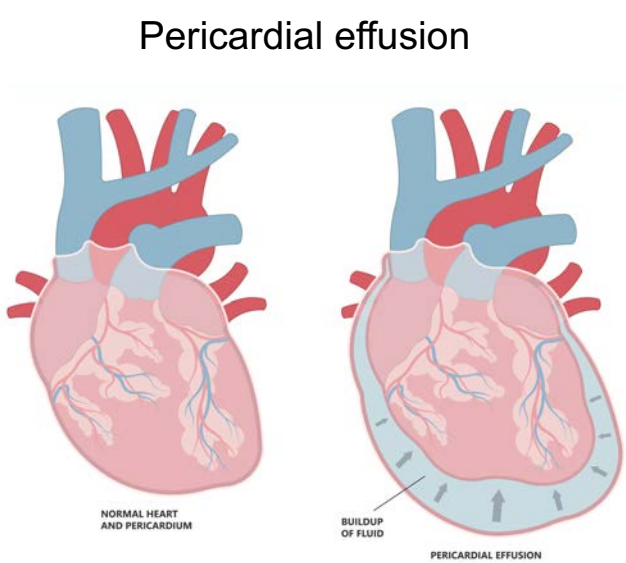

Figure 1. Healthy heart (left) and heart with pericardial effusion (right). (Licensed under Adobe Stock Standard license)

1.1.1 Pleural effusion

A pleural effusion is analogous to a pericardial effusion in that it accumulates between the two layers of the pleura, a double-layered sac comprised of connective tissue surrounding each lung. The same basic principles govern both

types of effusions, but they are not equivalent. Pleural effusions play a relatively small part in this thesis and will not be discussed in depth. A figure showing a healthy lung and a lung with a pleural effusion is shown in **Figure 2**.

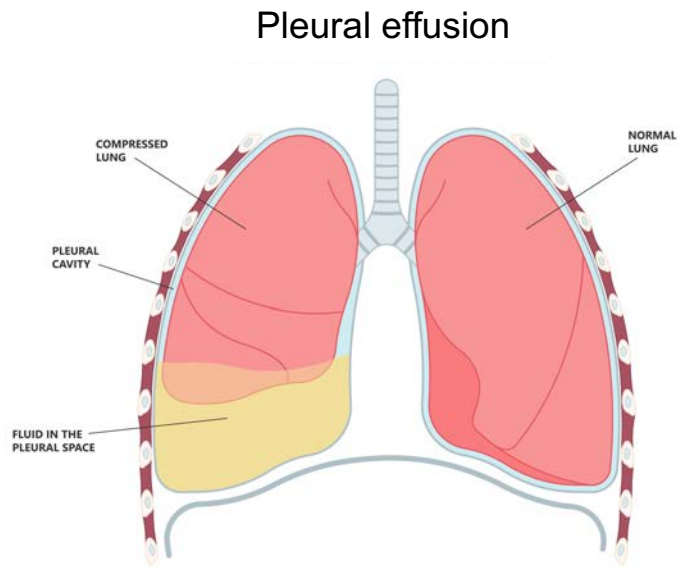

Figure 2. A lung with pleural effusion (left) and a normal lung (right). (Licensed under Adobe Stock Standard license)

1.1.2 Pathophysiology and Starling forces

Pericardial fluid is an ultrafiltrate of plasma. The equation governing the movement of fluid across a semipermeable membrane that follows from the principles of irreversible thermodynamics can be used to describe the movement of fluid across the pericardium:

$$\frac{J_v}{A} = L_p(\Delta P - \Delta\Pi) \tag{1-1}$$

where J_v is the volume filtration rate per unit endothelial area A, L_p the permeability coefficient, ΔP the difference in hydrostatic pressure and $\Delta\Pi$ the difference in osmotic pressure across the membrane (4). Writing out these differences in pressures yields the Starling equation that was first hypothesized in 1896 (5) and later experimentally confirmed (6,7):

$$\frac{J_v}{A} = L_p((P_c - \mathrm{P}_i) - (\Pi_c - \Pi_i))$$

(1-2)

where P_c and Π_c are the hydrostatic and oncotic pressures in the capillary, in our context specifically the capillaries of the pericardium, and P_i and Π_i the hydrostatic and oncotic pressures in the interstitium, in our context the pericardial space (4). Any process localized to or close to the heart causing inflammation may change the permeability of the pericardium and can be represented in Eq. (1-2) above as an increasing L_p, resulting in a larger net flow of fluid. Systemic processes such as elevated systemic arterial blood pressure seen in congestive heart failure, pulmonary hypertension, or kidney failure (3) can be represented in Eq. (1-2) as an increased P_c, also results in a larger net flow of fluid. Hypalbuminaemia, which occurs in liver cirrhosis or nephrotic syndrome, can be represented in Eq. (1-2) as a decreased Π_c, also results in a larger net flow of fluid (8). A traumatic injury to the heart, creating a direct connection between space within the heart and the pericardial space, can cause blood to accumulate (9). More rarely, chyle emanating from damaged lymphatic vessels may accumulate in the pericardial space (10). Furthermore, gas produced by bacteria or air from gastrointestinal fistulae, although not technically effusions, may become trapped within the pericardial space (11).

Pericardial effusion is usually classified based by its onset; acute, subacute, or chronic, anatomical distribution; circumferential or localized, hemodynamic impact; none, cardiac tamponade, effusive-constrictive, composition; exudate, transudate, blood, air or gas, and by the size of effusion as mild, moderate or severe (3). The clinical severity of pericardial effusion does not solely depend upon the amount of fluid, but also on the speed with which the fluid accumulates (12).

1.1.3 Epidemiology

Epidemiological studies of pericardial effusion can be considered lacking in comparison to its incidence and prevalence, as one study reported an incidence and a prevalence of pericardial effusion at 3% and 9%, respectively (12). Another study found that the most common diagnoses underlying pericardial effusion were; acute idiopathic pericarditis (20%), iatrogenic effusions (16%), cancer (13%), and chronic idiopathic pericardial effusion (9%). In 60% of cases, the cause of pericardial effusion was a known medical condition (13). A specific causative

agent is far from always found, and the disease is often classified as idiopathic. A pericardial effusion can occur any time the pericardium is damaged or compromised, and thus the aetiology of pericardial effusion varies greatly. Infection, neoplasm, autoimmune processes, metabolic processes, hypertension, liver failure, kidney failure, and drug toxicity are some of the underlying etiologies (13). Pericardial effusion also frequently occurs as a complication following cardiac surgery (11).

1.1.4 Transudates and Exudates

Pleural and pericardial effusions can roughly be divided into two categories related to their etiology. A transudate, usually a clear liquid, is the result of a systemic process whereby the pericardium, $L_p$is intact but hydrostatic forces, P and Π are altered. Conversely, an exudate, usually a proteinaceous opaque liquid, is the result of a local process, more specifically inflammation, where the permeability of the pericardium has been affected but the hydrostatic forces remain unchanged.

The difference is clinically significant because it informs the physician where the problem should be addressed. In the case of a transudate caused by renal failure, ideally, renal failure should be treated. In the case of an exudate due to infection, ideally, the infection is treated.

For pleural effusions, the Light criteria (14,15) and variations thereof (16) are used clinically to separate transudates and exudates biochemically. The classical Light criteria stipulate that a pleural effusion is likely an exudate if one of the following is true:

I. The ratio of effusion protein to serum protein is greater than 0.5
II. The ratio of effusion LDH and serum LDH is greater than 0.6
III. Effusion LDH is greater than 0.6 or two-thirds the normal upper limit for serum.

It is important to remember that, ultimately, the etiology determines whether an effusion is a transudate or exudate, not its biochemical composition. For example, a transudate effusion is caused by heart failure, and the patient receives diuretic treatment. Biochemically, due to the loss of water content in the fluid, the effusion can be falsely classified as an exudate (17), though in the correct sense, it is still a transudate.

The Light criteria were developed and validated for use in pleural effusions. While the same etiological separation between transudate and exudate applies to pericardial effusions. The biochemical cut-offs of the Light criteria do not (18) and some argue that biochemical analysis of pericardial effusion fluid has no diagnostic value (19).

The Diagnostic Challenge

If fluid accumulation is slow enough, the pericardium can stretch and become more compliant such that the volume of a chronic pericardial effusion can be measured even in liters. Inversely, a rapid yet small pericardial effusion can potentially cause cardiac tamponade (20). The feared end-stage of pericardial effusion, cardiac tamponade, occurs when the pericardial sac cannot stretch further, and the chambers of the heart are compressed. A decreasing chamber volume decreases diastolic compliance and limited cardiac inflow (8,9). Unless treated, cardiac output declines to shock and death (20). However, most patients with pericardial effusion do not develop cardiac tamponade, and identifying patients who are at risk is a challenge. The clinician cannot know in advance the amount of fluid that can be accommodated within the pericardium of the patient (1). In a follow-up study of patients who suffered from idiopathic pericardial effusion, one-third of patients developed cardiac tamponade unexpectedly (21).

A range of hemodynamic events can precede cardiac tamponade, all of which can, to some degree, inform the clinician of the hemodynamic significance of the pericardial effusion. The collapse of the right atrium, colloquially referred to as "atrial buckling," can occur during early systole. Right atrial collapse has a reported sensitivity of between 50% and 100% and a specificity of between 33% and 100% for the later development of cardiac tamponade (22). Another study found that observation of right atrial collapse during more than a third of the cardiac cycle is highly predictive of cardiac tamponade with a sensitivity of 100% and specificity of 94% (23). The collapse of the right ventricle can occur during early diastole when pericardial pressure exceeds right ventricular early diastolic pressure and has a reported sensitivity between 60% and 90% and a specificity of between 80% and 100% for the development of cardiac tamponade (24). Conversely, another study found that about one-third of patients with pericardial effusion but without cardiac tamponade had at least

one heart chamber collapse on the echocardiography (25). Further clinical signs of hemodynamic significance of pericardial effusion are discussed in 1.3.

1.1.5 Treatment

The first line of treatment for a pericardial effusion is to manage the underlying cause of the effusion. If the pericardial effusion is progressing towards cardiac tamponade, a procedure called pericardiocentesis is promptly performed, where a needle is inserted into the pericardial space and the fluid drained. For recurrent pericardial effusions, a pericardial window, a small patch of the outer pericardium, can be surgically removed (26).

1.2 Constrictive pericarditis

1.2.1 Pathophysiology

Constrictive pericarditis results from a chronic inflammatory process leading to a fibrous thickening, calcification, or both of the pericardium. This impairs the diastolic filling of the heart and reduces cardiac output, eventually causing heart failure (27).

1.2.2 Epidemiology and Diagnosis

Tuberculosis is the dominant cause of constrictive pericarditis in Africa, Asia, and South America, while in North America and Europe, previous chest surgery or radiation treatment of the chest has become a more common cause (28). It is also associated with systemic inflammation in various rheumatologic diseases (29).

Accurate and timely diagnosis is essential to differentiate constrictive pericarditis from other conditions with similar symptoms, such as restrictive cardiomyopathy. This differentiation is vital as the treatment and prognosis for these conditions differ significantly (30).

Doppler echocardiography, especially when performed with respiratory recording, is highly sensitive for diagnosing constrictive pericarditis. It predicts the functional response to pericardiectomy (31). Cardiac catheterization is sometimes performed, especially in complex cases where non-invasive methods provide conflicting data (31). Assessing the hemodynamics unique to constriction is beneficial because 18% of cases confirmed through surgery do not show pericardial thickening, necessitating hemodynamic evaluation (32). A

multiparametric CMR exam can detect pericardial inflammation, thickening, and effusion (33).

1.2.3 Treatment

Pericardectomy, a surgical procedure where the entire pericardium is stripped and removed, can cure constrictive pericarditis, but the procedure itself is associated with considerable mortality and morbidity (34). In cases of constrictive pericarditis with a significant inflammatory component, early intervention with anti-inflammatory therapy can be effective, potentially avoiding the need for surgery (35)

1.3 Ventricular Interdependence

During normal breathing, a negative intrathoracic pressure is caused by the lowering of the diaphragmatic valve. It creates a pressure gradient between the atmosphere and the lungs, driving air into the lungs. However, a pressure gradient is also created between the thorax and the rest of the body, which results in an increased venous return to the right side of the heart. As the total volume of the heart is relatively fixed, an increased venous return to the right side of the heart must cause a decreased venous return to the left side of the heart. More intuitively, the two sides of the heart can be considered competing for the same fixed volume, and any change in the volume of one side will cause the opposite change in the other (20). This occurs normally, but when fluid accumulates pericardial space or an inflamed pericardium constricts the heart, the level of competition increases. This phenomenon is called ventricular interaction or interdependence (36). Ventricular interdependence is the cause of pulsus paradoxus, an important clinical sign of hemodynamically significant constriction of the heart. It is defined as a drop of 10 mmHg in systolic blood pressure during inspiration. It was first described by Richard Lower in 1669 and was later termed "pulsus paradoxus" by Adolf Kussmaul in 1873 in patients with constrictive pericarditis. Ventricular interdependence is the underlying principle of the increased respiratory variation in transvalvular peak inflow velocities that are valuable clinical signs of the hemodynamical significance of a pericardial effusion (37).

Doppler echocardiography has demonstrated an increased respiratory variation in transvalvular peak inflow velocities in patients with pericardial effusion that were normalized after pericardiocentesis (38,39). One study has shown diminishing respiratory variation in mitral inflow velocity measurements before,

during, and after pericardiocentesis in patients with cardiac tamponade (40). Furthermore, increased respiratory variation in mitral inflow velocity was highly indicative of increased pericardial pressure measured invasively (41) and has also been studied using induced pericardial effusion in dogs (42). In the absence of cardiac tamponade, other respiratory effects of pericardial effusion on hemodynamic parameters have also been demonstrated, e.g., on systolic time intervals, left ventricle diameter, and ejection time (43–45).

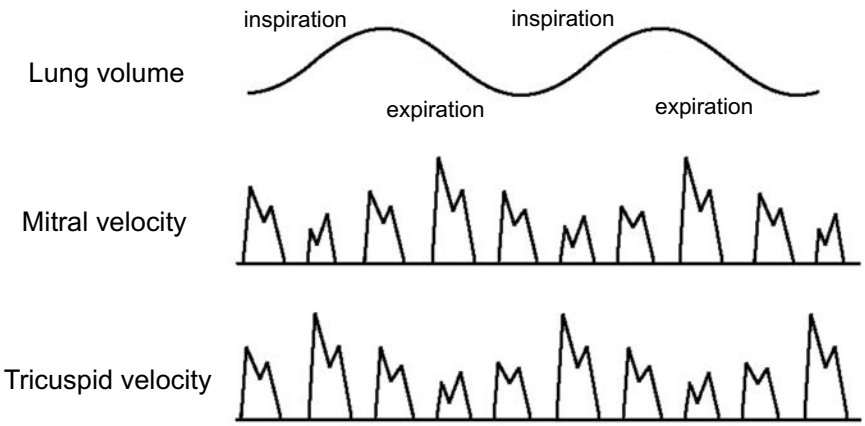

Figure 3. Schematic diagram of simultaneous lung volume during inspiration, expiration, and changes in inflow velocity across the mitral and tricuspid during cardiac tamponade.

Respiratory variation in transvalvular inflow velocities has also been studied in relation to constrictive pericarditis. The diagnosis of constrictive pericarditis remains a challenge, and respiratory variation in transvalvular inflow velocities measured using Doppler echocardiography is considered a valuable tool in separating constrictive and restrictive physiologies (4,13–15). Cardiovascular magnetic resonance imaging (CMR), using a RT-PC technique that can measure flow velocities in real-time, has been used to demonstrate an increased ventricular interdependence in patients with constrictive pericarditis as compared to normal controls (46). Another study using the same technique found that 92% of patients with definite constrictive pericarditis had an increased ventricular interdependence, but did not include controls (47).

The increases in respiratory variation in transvalvular inflow velocities seen in cardiac tamponade and constrictive pericarditis are related but not identical (48,49). Both result from an altered pressure-volume relationship in the heart

imposed by a pericardial effusion or a rigid thickened pericardium. In the case of constrictive pericarditis, an inflammatory process may lead to stiffness, which in turn decreases the ability of the pericardium to deform. In cardiac tamponade, a fluid build-up may already have stretched the pericardium to its limit (50). The increased ventricular interdependence in the case of constrictive pericarditis is caused by a decreased pulmonary venous return to the left ventricle during inspiration rather than an increased systemic venous return to the right ventricle as in the case of a pericardial effusion (16).

1.4 Magnetic Resonance Imaging

Nuclear magnetic resonance is the physical phenomenon upon which magnetic resonance imaging is based. It was first observed in 1938 in beams of molecules traversing a magnetic field (51), and later in 1944 in solids and fluids (52) and first used in 1971 to differentiate cancerous from healthy tissue (53) and in 1973 demonstrated as being capable of generating two-dimensional images (54).

1.4.1 Basic Imaging Physics

The question of why and how the signal that ultimately constitutes the image in MRI requires an answer based on quantum mechanics. However, it has been shown that the behavior of the actual signal does not (55). Therefore, we can thankfully set quantum mechanics aside and avoid much confusion by accepting that atomic nuclei have a quantum mechanical property called spin that gives rise to a magnetic moment. In this thesis, only the nuclei of the hydrogen atom, a single proton, will be considered for simplicity. The magnetic moment of hydrogen nuclei can be conceptualized as tiny bar magnets, each with a positive north pole and a negative south pole. Placed in an external magnetic field, the magnetic moment will precess around the external field with a frequency that is characteristic to the nuclei, known as the Larmor frequency ω, which is proportional to the field strength of B_0 as given by

$$\omega = \gamma B_0 \tag{1-3}$$

Where γ is the gyromagnetic ratio which is specific to the element in question as given by:

$$\gamma = \frac{q}{2m}$$

(1-4)

where q is its charge and m its mass.

We can describe the net magnetization vector as **M** = (M_x, M_y, M_z) in the presence of B_0 (56).

The magnitude of **M** is governed by a Boltzmann distribution, which is a probability distribution that gives the probability of a certain state as a function of that states energy and temperature of the system. In our system:

$$|\boldsymbol{M}| = B_0 \rho \frac{\gamma^2 \hbar^2}{4 k_B T}$$

(1-5)

where ρ is the spin density, $\hbar$ the reduced Planck constant, k_B is Boltzmann's constant and T the temperature.

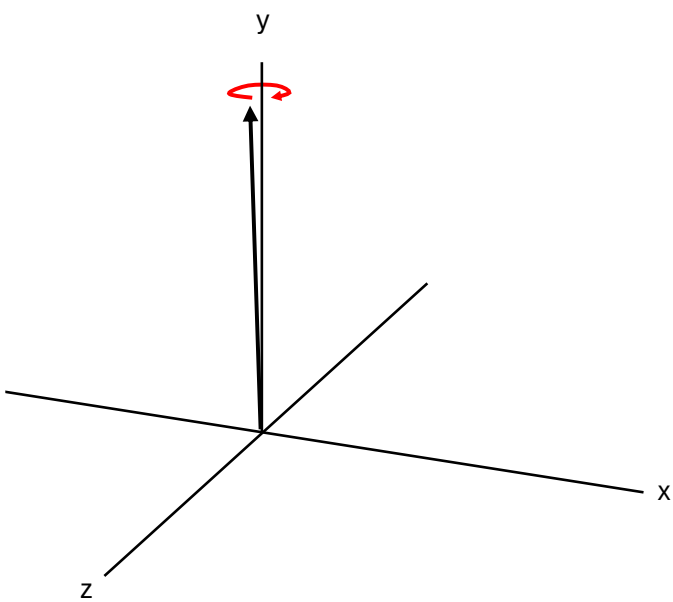

Figure 4. The three cartesian coordinate axes and the net magnetization vector M precessing. B_0 is in this case parallel to the y-axis.

1.4.2 Faraday Induction

We have not yet discussed how the image is formed but merely stated some of the underlying principles of nuclear magnetic resonance. Recall that the Faraday law of induction states that if a conductor circuit is placed within a time varying

magnetic field, a current is induced. The original Faraday experiment consisted of two coils, one connected to a battery and one to a voltmeter. Faraday showed that when moving one coil inside of the other, thus creating a time varying magnetic field, the voltmeter would detect a voltage as shown in **Figure 5**.

Now imagine a closed circuit consisting of a coil connected to a voltmeter placed in the plane is perpendicular to B_0 into which we have just tipped the net magnetization vector M. According to the Faraday law of induction, a voltage will be induced in the coil. In mathematical terms, Faraday's law of induction takes the form of:

$$V(t) = -\frac{\partial \Phi}{\partial} \tag{1-6}$$

Where V(t) is the induced voltage in the coil and Φ the magnetic flux through the coil. The expression $\frac{\partial \Phi}{\partial}$ is then the time-derivative of the magnetic flux, or in simpler terms, the change in the magnetic flux over time.

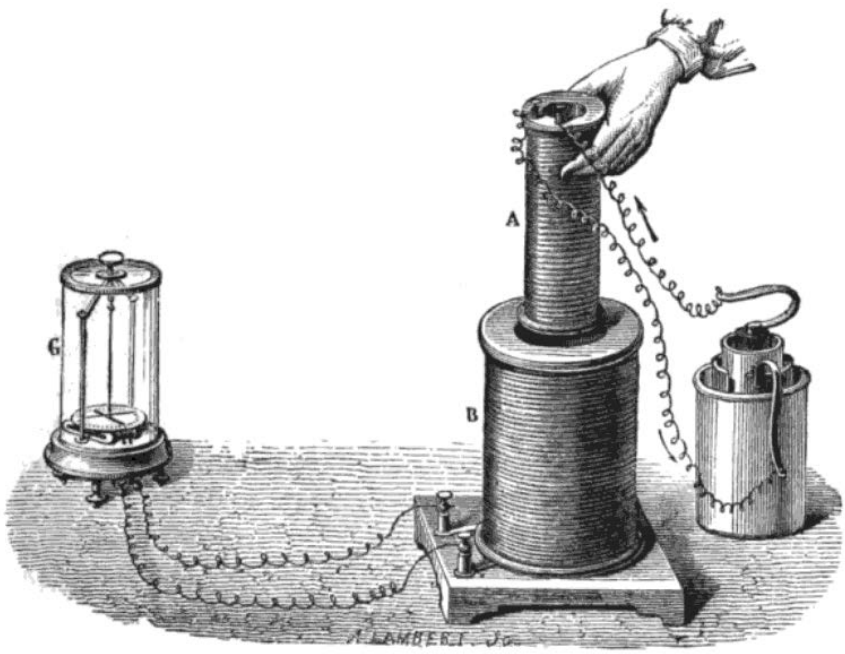

Figure 5. Drawing of an experiment demonstrating Faraday induction. On the right is a battery that creates a creating a magnetic field around the small coil of wire *(A)*. When the small coil is moved in or out of the large coil *(B)*, the change in magnetic flux induces

a current in the large coil. This is detected by the deflection of the needle in the galvanometer *(G)* on the left. Original drawing by Lambert J, distributed under a CC BY-SA 4.0 license.

This is how the signal is recorded in the MR scanner. It is generated in the coils in the scanner by Faraday induction when the net magnetization vector is rotating in the M_{xz} plane.

1.4.3 The Concept of Resonance

Resonance is a concept intuitively understood by anyone who has learned to ride a swing. Consider the pendulum that is a swing, it moves forward and backwards when pushed. If it is pushed regularly with a series of pushes its motion can be built. However, the person pushing must take into consideration the frequency of the pendulum that is the swing. If pushed regularly when moving towards the person pushing, motion will be decreased, but if pushed when moving away, motion is built. If pushed regularly but out of sync with the swinging pendulum, motion will be decreased or increased depending on where in the swinging motion the push occurs. Resonance thus does not occur. If the pushes are delivered regularly and in sync with the swinging motion of the pendulum, even a gentle push can build and maintain the swinging motion.

1.4.4 Achieving Rotation in the M_{xy} Plane

To induce a current in the coils, the magnetization vector **M** needs to have x and y components. Here is where the concept of resonance is comes in. Keeping this concept of resonance in mind, picture what the effect of a magnetic field B_1, rotating at the Larmor frequency, called B_1, is described by:

$$\boldsymbol{B}_1(t) = B_1^e\left(\cos\left(\omega_{rf} + \phi\right)\hat{x} - \sin\left(\omega_{rf} + \phi\right)\hat{y}\right) \tag{1-7}$$

Where B_1^e is a scalar function called the pulse envelope function, ω_{rf} the excitation carrier frequency in a plane perpendicular to B_0 would have on the net magnetization vector **M**. The effect would be that **M** would tip and start to align with the plane perpendicular to B_0, the xy-plane, even though B_1 is a much weaker magnetic field than B_0. In a pendulum analogy it is difficult to push a swing to 90° in one push, exploit resonance and gradually push the pendulum and it can easily be achieved. B_1 is often referred to as the radio frequency (RF)

pulse. It is a rotating magnetic field and only protons precessing at the same frequency as the rotation of the magnetic field will be affected by it.

1.4.5 T1 relaxation, T2 decay and Free Induction Decay

When the net magnetization vector has been oriented into the xy-plane it will return to its initial equilibrium state. This happens by two processes that are independent of each other. The longitudinal component of the net magnetization vector, or the z component, denoted **Mz**, will relax back to its equilibrium state value. This is called T1 relaxation and the time it takes for it to regain 63% of its equilibrium state value is called the T1 time constant or T1 for short.

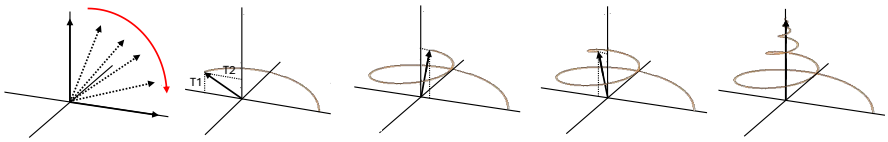

Figure 6. The net magnetization returns to thermal equilibrium after having been tipped by a rotating magnetic field.

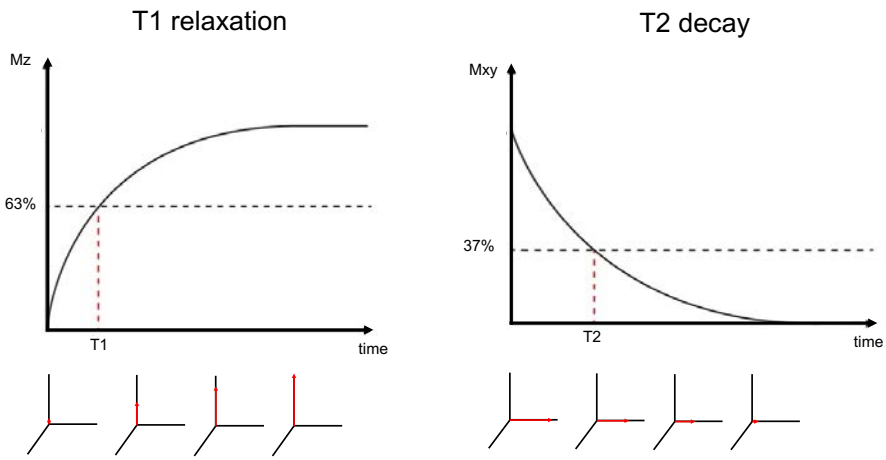

Figure 7. Illustrations of T1 relaxation and T2 decay. The time it takes for the longitudinal z-component of the net magnetization vector to increase to 63% of its equilibrium state value is called the T1 time constant. The process is called relaxation and is independent of T2 decay. The time it takes for the transverse xy-component of the net magnetization vector to decay such that 37 % is remaining, as it decays towards 0 is called the T2 time constant.

T1 is the rate at which M_z, the longitudinal component of the net magnetization vector recovers exponentially and is described by:

$$M_z(t) = M_{z,eq} - (M_{z,eq} - M_z(0))e^{-t/T1}$$

(1-8)

Where $M_{z,eq}$ is the M_z at the equilibrium state.

Different tissues have different T1, which can be create contrast in an image.

Likewise, T2 is the rate at which M_{xy}, the transversal component of the net magnetization vector decays exponentially and is described by:

$$M_{xy}(t) = M_{xy}(0)e^{-t/T2}$$

(1-9)

Usually in MRI some combination of T1 and T2 is measured. There are a plethora of techniques to perform T1-weighted or T2-weighted imaging, where the contrast consists of different T1/T2 values that correspond to different tissues.

1.4.6 Significance of Fourier analysis

Fourier analysis is a method for breaking down a complex signal, such as a sound or image, into its individual frequency components. The basic idea is that any complex signal can be represented as a sum of simpler sinusoidal waveforms of different frequencies, amplitudes, and phases. It is a sort of mathematical decomposition that transforms data from the spatial image domain into the frequency domain. A more graphical and intuitive explanation is given in **Figure 8**.

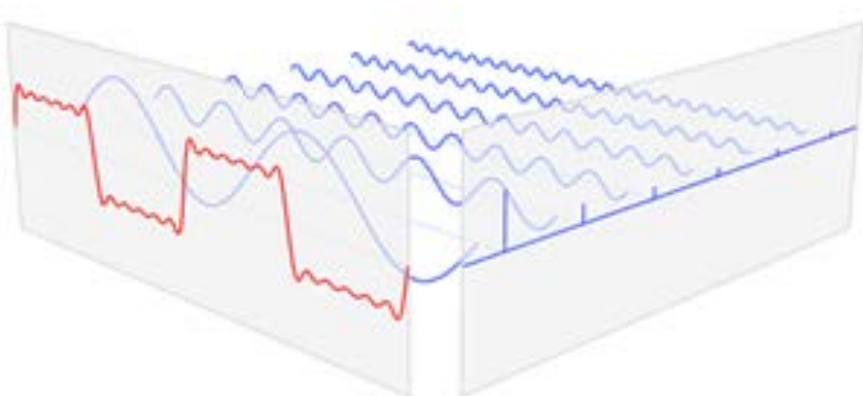

Figure 8. An example of how a signal, red curve here seen in a time (x-axis) plotted against amplitude (y-axis), can be represented by several sine and cosine waveforms of different frequency, amplitude and phase (collection of blue curves). The red graph is the sum of all the blue graphs. The blue graph on the right is instead a graph of amplitudes (y-axis) plotted against frequency (x-

axis). The Fourier transform and its inverse are means to move from one to the other.

1.4.7 Significance and Proof of Euler's Formula

Fourier showed that any signal can be represented as a combination of sine waves. Sinusoidal functions can be more succinctly expressed as the sum of exponential functions with imaginary exponents. This is because of Euler's formula which states that for all real numbers x:

$$e^{ix} = \cos x + \mathrm{i}\sin x \tag{1-10}$$

This formula is fundamental in the field of complex numbers and is crucial in understanding wave-like phenomena. In MRI, the signals that are used to create an image are essentially wave-like. This identity is so ubiquitous in mathematics and physics was that it was coined "our jewel" by legendary theoretical physicist Richard Feynman in one of his lectures (57). It provides a link between the natural logarithm, complex numbers, and trigonometry.

The proof of this equality is remarkably simple and its beauty is available to anyone familiar with the product rule of differentiation and some elementary arithmetic.

Consider the function $f(x)$ where $x \in \mathbb{R}$

$$f(x) = \frac{\cos x + i \sin x}{e^{ix}} \tag{1-11}$$

Which can be rewritten:

$$f(x) = e^{-ix}(\cos x + i \sin x) \tag{1-12}$$

Differentiating $f(x)$ using the product rule gives us:

$$f'(x) = e^{-ix}(\cos x - i \sin x) - ie^{-ix}(\cos x + i \sin x) = 0 \tag{1-13}$$

A function that has a zero derivative is trivially constant, thus $f(x)$ is constant and since $f(0) = 1$, then $f(x) = 1, \forall x \in \mathbb{R}$ and thus we arrive at eq. (1-11):

1.4.8 Slice Selection, Phase and Frequency Encoding

The scanner is capable of creating gradient magnetic fields within the bore such that the magnetic field is stronger at one position compared to another. These gradient magnetic field are used to spatially locate the signal received, or to encode the position in the signal. Paul Lauterbur and Peter Mansfield shared the Nobel prize in medicine and physiology for this discovery in 2003.

When a gradient magnetic field is applied along one axis of the patient's body. This gradient causes a linear variation in the magnetic field strength along that axis, this affects the Larmor frequency of the hydrogen nuclei as described in Eq. (1-3. The carrier frequency of the RF pulse is tuned to the frequency at the location of interest. Only hydrogen nuclei in that thin slice will be tipped into the xy-plane. Only there do we achieve resonance between hydrogen nuclei and the RF pulse. This is called the slice selection gradient.

After the slice selection, another gradient field is applied along a second axis. This gradient again changes the Larmor frequency of the hydrogen nuclei along the second axis. When turned off, this will cause a difference in phase along that axis. This is called the phase encoding gradient.

Finally, a third gradient is applied during the signal acquisition along the third axis, which causes the hydrogen nuclei to process at a frequency proportional to their position along that axis. This is called the frequency encoding or readout gradient.

The net result is that a thin slice of hydrogen nuclei has been tipped into the xy-plane, and the frequency and phase of the signal they generate in the receiver coils can be used to localize the origin of the signal.

The details of pulse sequences are often represented as a diagram. It specifies how the RF pulse and the three gradients change and when the signal is recorded.

In CMR, a balanced steady state free precession (bSSFP) pulse sequence is often used. The most essential quality of the bSSFP sequence is that it is fast. This is a requirement when imaging the heart as the heart is both deforming while beating and pushed up and down by the diaphragm during breathing. A standard CMR exam includes cine imaging, where images are acquired continuously during several cardiac cycles and averaged together to form a movie that captures

movement and changing volumes in the heart. The bSSFP pulse sequence diagram is shown in **Figure 9**.

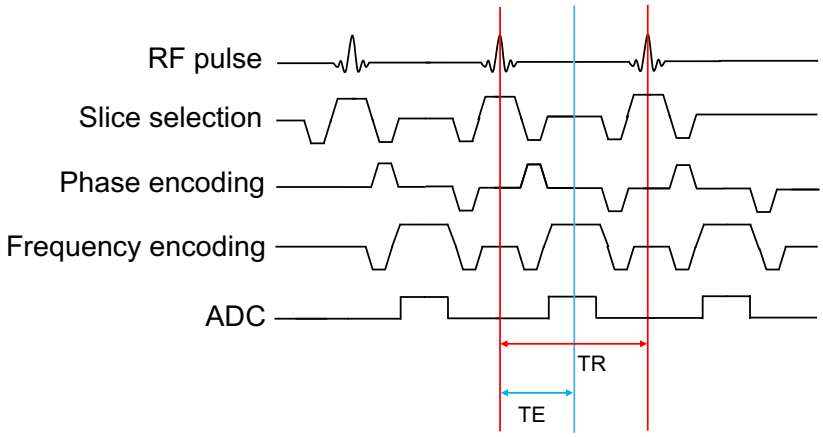

Figure 9. A pulse sequence diagram showing the bSSFP pulse sequence. RF is the RF pulse used to tip the net magnetization vector. The slice selection, phase encoding and frequency encoding gradients are shown. ADC indicates when the analog to digital converter is turned on i.e. when we record the induced voltages in the coils, the so called echo. TR is the repetition time of the sequence and TE the time after the RF pulse until the echo is formed.

Having played out a number of repetitions of the pulse sequence in **Figure 9** we have now recorded many sine waves formed by the net magnetization vector rotating and inducing a voltage in the coils. Each sine wave is completely described by its amplitude, frequency and phase. At this stage, the recorded signals are usually represented in k-space form. k-Space is the raw signal data, i.e., the amplitudes, frequency and phases of the sine waves. It is named k-space because by convention, k is the name of a term in the equation describing signal. k Denotes spatial frequency and has three components: kx, ky, and k_z. k-Space is usually described visually as a plot of the magnitude at each point in k-space and uses as its axes the spatial frequencies k_x, k_y and k_z.

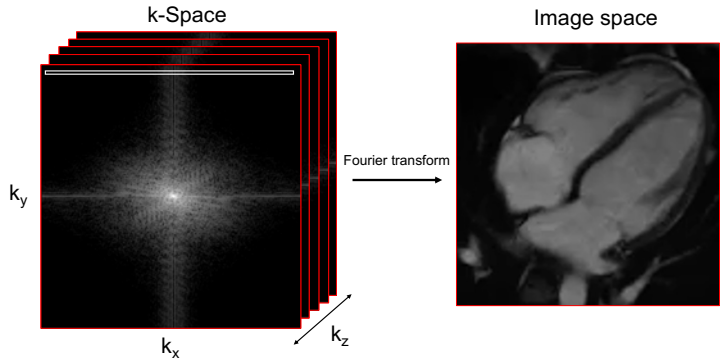

Figure 10. An example of k-space and image space representations of a cardiac 4-chamber view. The white rectangle represents one repetition time (TR) of the sequence. Usually, one repetition of the pulse sequence will acquire one line in k-space. In what manner k-space is acquired is called a trajectory. Reading in a straight line parallel to an axis is called a cartesian trajectory.

Applying the Fourier transform on the k-space representation of the signals is equal to mapping the amplitudes, frequencies, and phases onto signal intensities on a cartesian grid, an image. Every point in k-space contributes to each pixel in the image.

1.4.9 T1 mapping

Depending on the specifics and timing of the radiofrequency pulse used to change the alignment of the protons, images where differences in T1 constitute the contrast to a varying degree can be created. Such images are called T1 weighted images and can be used to qualitatively assess the relative T1 of parts of the image. The principle for T1 mapping is to acquire several images with varying amounts of T1 weighting and fit the signal intensities to the exponential function describing the recovery of the longitudinal magnetization component in Eq. (1-8. Several techniques for acquiring T1 maps exist, each with advantages and disadvantages (58,59). The most clinically used T1 mapping sequence is the modified Lock-Locker inversion recovery (MOLLI) sequence. Instead of the net magnetization vector being tipped by 90° into the xy-plane, it is possible to keep going and flip the full 180°. After being flipped, the net magnetization vector will undergo T1 relaxation and we can sample points along the T1 relaxation curve shown in **Figure 7**, using a bSSFP sequence. After we have performed the curve fit for each pixel in the image, we have a quantitative map of the T1 values of the tissue. Slight variations of the MOLLI pulse sequence exist. A schematic of the most clinically used MOLLI pulse sequence variant is shown in **Figure 11**.

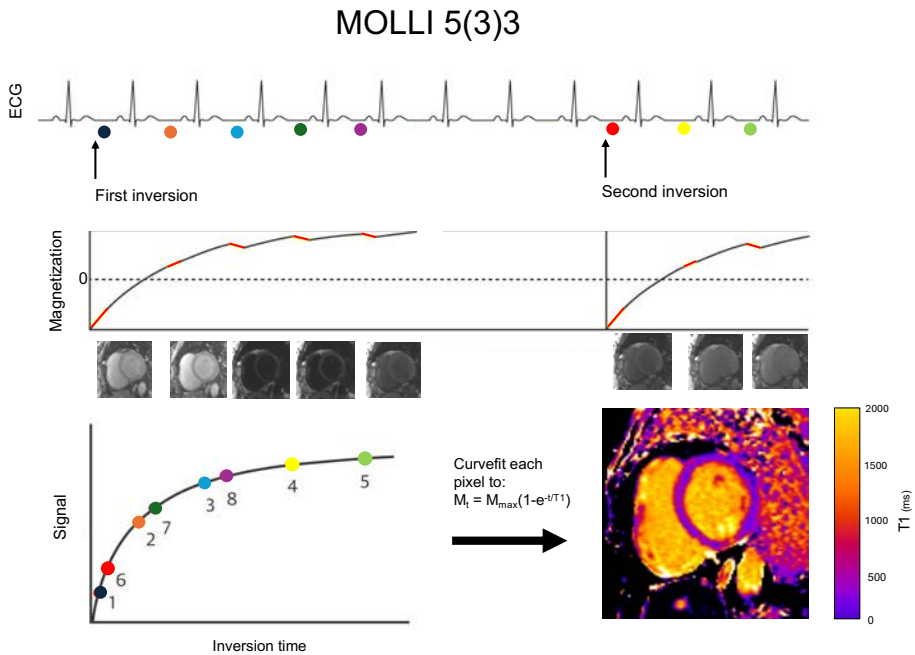

Figure 11. A schematic of the MOLLI 5(3)3 pulse sequence. Each step is triggered by an ECG. An inversion is made, the T1 sampled five times in diastole followed by a three heartbeat pause. A second inversion is made and the T1 sampled three times in diastole. The images are sorted in terms of time passed after an inversion. Each pixel in the image is curve fit to the T1 relaxation equation.

Besides providing valuable information in and of itself, T1 mapping can be used to measure the percent of tissue comprised of extracellular volume (ECV), which represents the fraction of tissue comprised of extracellular space in percent. This is a more physiologically intuitive unit of measurement compared to the time constant T1 measured in units of time, typically milliseconds. The basic principle behind measuring ECV is to acquire T1 maps before and after the injection of a gadolinium-based contrast agent (GBCA). ECV can then be estimated from the concentration of extracellular contrast agent in the myocardium relative to the extracellular space in blood determined in the image and from a blood sample (60).

1.4.10 Excretion of Contrast Agents

Both computerized tomography (CT) and MRI make use of contrast agents. The basic principles governing the contrast agents used in CT and MRI are effectively the same and involve intravenous injection, extracellular distribution, and renal

excretion (61). Non-renal excretion, or vicarious excretion, has been described as a rare occurrence of limited or no importance. Non-renal excretion of both iodinated contrast agents and GBCA into a wide variety of anatomical spaces has been described in (62–69). Notably, T1 mapping is a technique that is much more sensitive for detecting small amounts of GBCA compared to conventional T1 weighted imaging. Furthermore, T1 mapping can quantify changes in contrast agent concentration in various tissues including pericardial fluid. However, no such systematic studies have been performed to date. It is unknown whether such characterization of contrast dynamics has any diagnostic value.

1.4.11 Phase Contrast Velocity Encoded Imaging

MRI can also be used to measure the velocity of tissue or blood using a phase contrast technique whereby the signal is proportional to the velocity of the tissue in question.

Phase contrast imaging relies on the fact that it is possible to encode velocity in the signal such that the phase shift of the precessing hydrogen nuclei will be proportional to the velocity. Sequential bipolar gradients are used to generate a flow encoding gradient that is applied after excitation but prior to the readout phase along the spatial direction of interest. This causes nuclei moving along that direction to gain phase proportional to their velocity. The first positive gradient de-phases the nuclei, whereas the second negative gradient re-phases them. A nuclei that is static will return to its initial un-phased state, whereas a moving nuclei will have accumulated a net phase shift proportional to its velocity.

Since the phase is limited to values between 0 and 2π, the operator must specify what the range of velocities to be measured should be. The operator specifies the velocity encoding gradient (VENC) corresponding to the maximum velocity expected to be measured. If the true velocity is greater than the VENC, aliasing will occur where the measured velocity will be given in modulo 2π. Increasing the VENC decreases the velocity-to-noise ratio. An example of aliasing is shown in **Figure 12**.

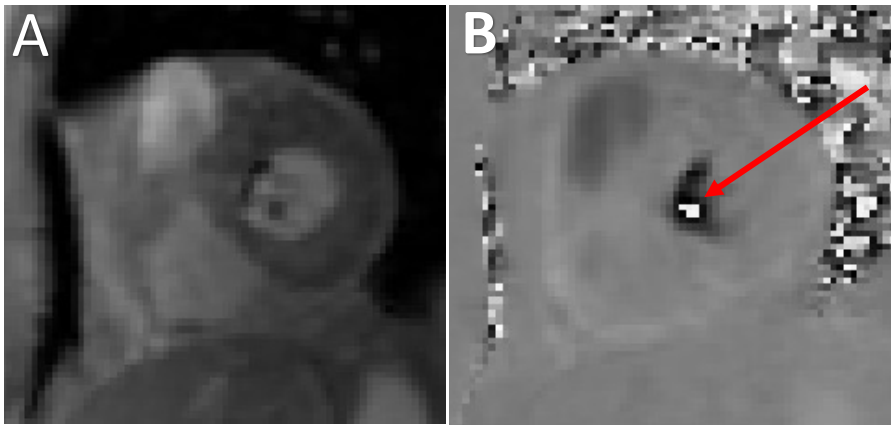

Figure 12. An example of aliasing in phase contrast imaging. Panel A shows a short axis view magnitude image, panel B show short axis view phase image. The red arrow indicates five pixels where aliasing has occurred.

Thus the RT-PC technique makes measurements of velocities of blood flow or tissues possible (70). Several studies have compared *in vivo* blood flow velocities within the heart by RT-PC and Doppler echocardiography. Generally, RT-PC has an excellent concordance with echocardiography (71–75).

1.4.12 Eddy Currents

Because magnetic resonance imaging involves rapidly shifting radiofrequency pulses and gradients, we are working with a time-varying electromagnetic field which, according to Faraday's law of induction, will give rise to currents in what we are imaging. These are called eddy currents and, in terms of phase contrast imaging, can cause errors of up to 3-4 cm/s when using a VENC of 150 cm/s.

One way the effects of eddy currents can be mitigated is stationary tissue background correction. Since we know which anatomical structures are stationary during imaging, we can estimate the effect of the eddy currents in an image and correct it. This first involves identifying which pixels in the image are stationary, and this can be automatically done by selecting a threshold of phase deviation in the phase image. A linear or quadratic surface is fitted and used to correct the phase in the original image. An example of this is presented in **Figure 13**.

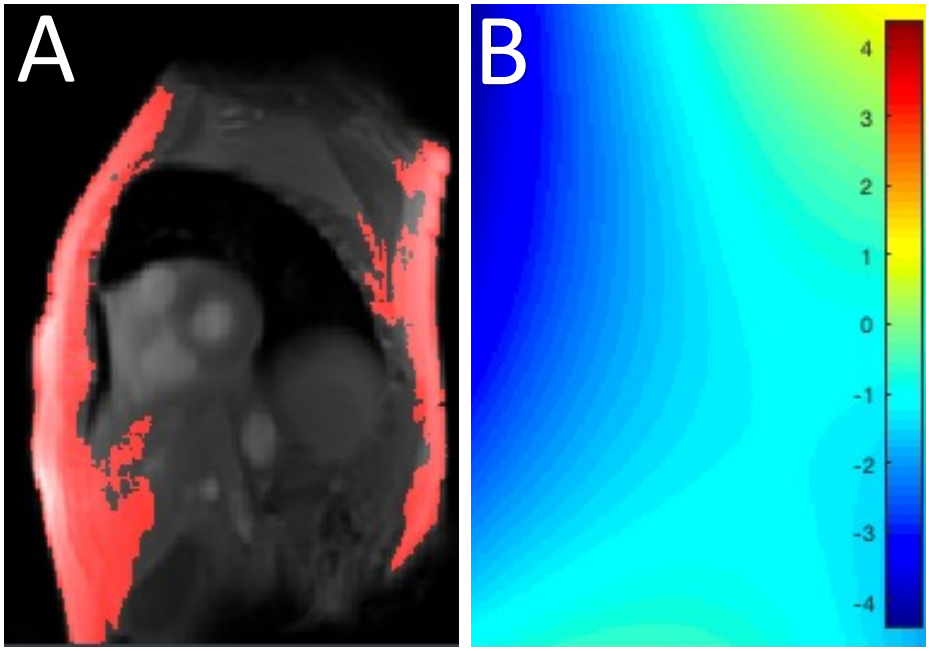

Figure 13. An example of eddy current compensation using static tissue background correction. Panel A shows pixels marked as stationary by having a phase deviation below a certain threshold. Panel B shows the quadratic surface used to correct the phase image.

1.5 Repeatability, Reproducibility, Agreement and Bias

The repeatability and reproducibility of a clinical measurement are crucial for its clinical usefulness. Repeatability refers to the consistency of a measurement when the same methods and conditions are applied repeatedly in a span of time. Reproducibility, on the other hand, involves obtaining consistent results under changed conditions, such as different operators or equipment. These aspects are fundamental because they ensure that a measurement is reliable and can be trusted in clinical settings. Without repeatability and reproducibility, the validity of any measurement method is questionable, rendering its application in clinical decision-making risky and potentially ineffective. Therefore, these characteristics are desirable and essential for any clinical measurement to be considered useful.

There is much confusion in the medical literature regarding the meaning of these concepts and reproducibility. In many cases in the literature, interstudy reproducibility, interstudy reliability, or even interstudy variability is used to mean repeatability. The meaning of inter- and intra-observer reproducibility is

dependent on the context. In some studies, the observer is the person performing the actual exam; in others, it is the person analyzing the data collected during the exam. Observer can, in this case, be replaced by rater, reader, or study for a plethora of study designs. However, repeatability and reproducibility have proper definitions in the measurement error subfield of statistics. In short, repeatability; same conditions, reproducibility; other conditions.

Consider a CMR exam, to be clinically useful, its measurements must be repeatable and reproducible. Repeatability in this context means that if the same patient undergoes several CMR exams in a short period under identical conditions, the measurements, such as ventricular dimensions or ejection fraction, should be consistent. Reproducibility means that these measurements remain consistent even when the CMR images are analyzed by different readers, physicians, or using different analysis software.

Without such consistency, a cardiologist cannot reliably track a patient's progress or make accurate diagnoses, thereby limiting the clinical utility of CMR as a diagnostic tool.

In medicine, measurements of quantities like pressure, volume, or velocity are challenging. Many measurements are indirect, as direct measurement can be harmful or impossible. New methods of measurement continuously arise, and evaluation of these is paramount before clinical adoption.

No method, including the current gold standard, is free from measurement error, therefore there will always be some disagreement between methods. There is no universal criterion for an acceptable level of disagreement between methods, and a clinical judgment is therefore always required. The situation is analogous to what constitutes an acceptable level of risk. Statistical methods cannot determine this. Ideally, the criteria for a satisfactory agreement should be defined in advance.

Agreement is a measure of how close two measurements made on the same subject are; ideally, it is measured in the unit of the measurement itself. This makes the above-mentioned judgment, whether the agreement is satisfactory or not, much easier to make. The usual way of quantifying agreement is to calculate the bias and 95% limits of agreement, as proposed by statisticians Bland and Altman (76).

The bias is simply the mean of the difference between all pairs of measurement. The 95% limits of agreement mean that based on the current measurements, future measurements are expected to lie within the limits in 95% of cases.

In the case of repeatability, the coefficient of repeatability is often used. It is analogous to the concept of bias and the 95% limits of agreement. Essentially, if the same measurement is repeated under the same conditions at a different time, we would anticipate that in 95% of cases, the difference between the repeated measurements would not exceed the coefficient of repeatability.

Other ways of expressing agreement exist, and some are used in this thesis. The intraclass correlation coefficient (ICC) has the advantage of ranging from 0, no reliability or agreement to 1, perfect reliability or agreement. This means measurements in different units can be compared, although such a comparison is not always meaningful. There are several types of ICC depending on the experimental design; a one-way random effects model is used when the same set of raters rates different subjects, whereas the two-way random effects model is used when subjects are rated by different sets of randomly chosen raters (77).

2 Aims

I. To investigate and compare the differences in T1 mapping characteristics and extracellular GBCA excretion dynamics in pleural and pericardial effusions.

II. To determine the feasibility of T1 mapping measurements in the pericardial fluid in healthy volunteers and establish normal values for native T1 and GBCA contrast excretion.

III. To develop a user-friendly method to measure diastolic ventricular interdependence by quantifying the respiratory variation in mitral and tricuspid early inflow velocities using semi-automatic analysis of RT-PC CMR images and derive normal reference values.

IV. To determine the test-retest reliability and inter-observer reproducibility of the method developed in III.

3 Materials and Methods

3.1 Study Populations

The study population for studies I and III were all consecutive patients with a clinical indication to perform a CMR exam at the Karolinska University Hospital, Stockholm, Sweden. **Study II and IV** included healthy volunteers who were recruited to perform a CMR exam. Ethical approval was granted for all studies, and all subjects timely provided written informed consent.

In **Study I**, patients who had undergone a contrast enhanced CMR exam for clinical evaluation of known or suspected heart disease to Karolinska University Hospital, Stockholm, Sweden between September 2013 and November 2015, who had provided written informed consent to participate in CMR research were screened for inclusion (n=1338). Inclusion criteria were at least 5 mm pericardial effusion and/or 5 mm pleural effusion in an end-diastolic cine 4-chamber image and T1 maps acquired in the same imaging slice before, early (approximately 3 min) and late (approximately 25 min) after administration of extracellular GBCA (0.2 mmol/kg, gadoteric acid, Dotarem®, Gothia Medical AB, Billdal, Sweden). Exclusion criteria were an incomplete exam, missing patient characteristics, and unevaluable image quality for imaging. A total of 55 patients were excluded. The final analysis included 69 patients with pericardial effusion, 54 with pleural effusion, and 12 with both. Patient characteristics are summarized in **Table 1** and **2**.

Table 1. Baseline variables for the pericardial and pleural effusion groups

Characteristics	Pericardial effusion		Pleural effusion		p-value
Number, n	69	*	54	*	
Age, years	58	(46-65)	64	(52-71)	0.03
Male sex, n (%)	41	(59)	32	(59)	0.82
LVM, g	187	(153-240)	188	(143-236)	0.82
LVMI, g/m2	97	(83-120)	95	(83-120)	0.79
LVEDV, mL	156	(127-190)	150	(125-190)	0.72
LVEDVI, mL/m^2	81	(69-88)	81	(65-100)	0.60
LVEF, %	47	(36-56)	44	(30-53)	0.22
BMI, kg/m^2	25	(23-28)	25	(22-29)	0.52
Effusion size, mm	8	(5-9)	14	(6-10)	<0.001

Continuous data are given as median (interquartile range) or number (%). LVM, left ventricular mass; LVMI, left ventricular mass index; BMI, body mass index; LVEDV, left

ventricular end-diastolic volume; LVEDVI, left ventricular end-diastolic volume index; LVEF, left ventricular ejection fraction; LVM, left ventricular mass; LVMI, left ventricular mass index. * n=12 had both a pericardial and a pleural effusion.

Table 2. Distribution of diagnoses by type of effusion

Diagnosis	Pericardial, *n (%)*		Pleural, *n (%)*	
Otherwise normal	3	(4)	2	(4)
IHD	21	(30)	18	(33)
Dilated LV	14	(20)	8	(15)
LVH	2	(3)	1	(2)
Dilated LV+LVH	2	(3)	1	(2)
Myocarditis	5	(7)	4	(7)
Tumor	2	(3)	0	
Reduced LVEF	3	(4)	3	(6)
Takotsubo	4	(6)	6	(11)
Pericarditis	3	(4)	3	(6)
Sarcoidosis	2	(3)	0	
Amyloidosis	2	(3)	3	(6)
Other	6	(9)	5	(9)
Total	69	(100)	54	(100)

IHD, ischemic heart disease; dilated LV, dilated left ventricle; reduced LVEF, reduced left ventricular ejection fraction, without ischemic heart disease or myocarditis; LVH, left ventricular hypertrophy; other, other diagnosis, such as vasculitis, postpartum cardiomyopathy, or indeterminate diagnosis.

In **Study II**, healthy volunteers (n=30) with an absence of history of cardiovascular disease were prospectively recruited. Clinical assessment of CMR images was used to confirm the absence of myocardial or pericardial disease. The exclusion criterion was metallic implants not safe for MRI. CMR imaging took place between August 2019 and December 2019 in the Department of Clinical Physiology, Karolinska Universitetsjukhuset, Stockholm, Sweden.

In **Study III**, patients (n=27) who had undergone a CMR exam for clinical evaluation of known or suspected heart disease at Karolinska University Hospital, Stockholm, Sweden, between May 2020 and October 2020, who had provided written informed consent to participate in CMR research were included.

In **Study IV**, healthy volunteers (n=15) without a history of cardiovascular disease were prospectively recruited. Clinical assessment of CMR images was used to confirm the absence of myocardial or pericardial disease. CMR imaging took place between October 2021 and December 2021 in the Department of Clinical

Physiology, Karolinska Universitetsjukhuset, Stockholm, Sweden. Exclusion criteria were any history of cardiovascular pathology or general contraindications to CMR.

3.2 Ethical Considerations

All studies were performed with ethical permits in place and in accordance with the declaration of Helsinki.

Some considerations are common to all study populations. Medical research involves the transfer of images and medical information outside of the hospital setting. Images are frequently transferred to personal computers for image analysis and statistics performed on spreadsheets. This raises ethical concerns as it can jeopardize the participants' personal integrity, which is protected by law. The standard practice in the field is pseudo-anonymizing all participant data before transfer. Pseudo-anonymization means each subject is given a participant number, and a key with matching participant number and participant identity is created. This key is kept behind a firewall in the safety of the research facility. A complete anonymization is not performed as any pathology discovered during image analysis needs to be traced back to the participant's personal identity to facilitate potential medical referral. All studies in this thesis adhered to this practice.

In **Study I and III**, patients with significant clinical conditions were retrospectively enrolled. This raises ethical concerns. The role of informed consent in this case cannot be overemphasized. Care needs to be taken to inform the patient that participation in this type of research does not affect their clinical care and, similarly, that declining to participate also does not.

Studies I and II involve using GBCA in patients and healthy volunteers. GBCAs are generally considered safe, evidence is documented in several studies that gadolinium deposition in brain structures like the basal ganglia and cerebellum can occur after repeated use (78). The evidence consists solely of relative T1 signal hyperintensity in these structures. Studies have shown a higher deposition of after linear gadolinium chelates compared to macrocyclic contrast agents (79). This finding suggests that the structure of the GBCA plays a significant role in how long gadolinium remains in the body. Although elemental gadolinium has been detected in tissue samples in patients administered the linear GBCA gadodiamide, no histological lesions were found (80). Neonatal and juvenile rats

receiving comparatively high doses of the linear GBCA gadobenate dimeglumine did not develop any pathologies (81). Several studies have not detected hyperintensity after serial injections with a macrocyclic GBCA (82–86). Only in one study, and only after more than four injections, was hyperintensity detected (78) and this result has not been replicated to date. The GBCAs used in **Study I and II** were all macrocyclic.

In 100,000 patients who received at least one clinical dose of GBCA, one study found no increased risk of developing parkinsonism, usually associated with the basal ganglia (87). Likewise, albeit small, another study in patients who had received over 20 administrations of gadolinium contrast showed no cerebellar pathology (88). No symptoms can be attributed to the administration of GBCA despite more than 450 million intravenous administrations occurring worldwide (89,90). While gadolinium deposition in the brain and other tissues is an observed phenomenon, its lack of association with clinically significant outcomes, safety profile in individuals with normal renal function, and the significant benefits of MRI research, all support the argument that using GBCA in research, even in healthy volunteers, is ethically sound. Furthermore, this is supported by medical society guidelines (91,92).

3.3 Cardiovascular Magnetic Resonance Imaging

The CMR protocols used in this thesis included an initial localizer sequence and 2-, 3-, and 4-chamber bSSFP cine images of the left ventricle, as well as a complete short-axis stack covering the entire heart. Typical imaging parameters included FOV 380x320 mm^2, matrix size 265x142 pixels with 1.5x1.5 mm^2 in-plane resolution, slice thickness 6 mm, bandwidth 930 Hz, repetition time/echo time 2.78/1.16 ms.

3.4 T1 Mapping

T1 mapping was used in **Study I and II** using a MOLLI pulse sequence (93). Images were acquired using a non-selective inversion pulse, balanced steady-state free precession single shot read-out at end-diastole. In **Study I**, MOLLI 5(3)3 with two inversions were made, five images acquired after the first inversion, followed by a three heartbeats pause, and three images acquired after the second inversion.

In **Study II**, T1 mapping used MOLLI 5s(3s)3s with two inversions; five images were acquired after the first inversion, followed by a three-second pause, and three images were acquired after the second inversion.

Typical image acquisition parameters included: flip angle 35°, matrix size 256 × 136–158, slice thickness 8 mm, initial inversion time 129 ms, field of view 300-410 × 241–384 mm2, parallel imaging factor 2.

In **Study I**, T1 mapping was performed according to clinical routine, a short-axis stack encompassing the entire myocardium before, early before (approximately 3 min), and late (approximately 25 min) after administration of an intravenous GBCA (0.2 mmol/kg, gadoteric acid, Dotarem®, Gothia Medical AB, Billdal, Sweden). Example T1 maps are shown in **Figure 14**.

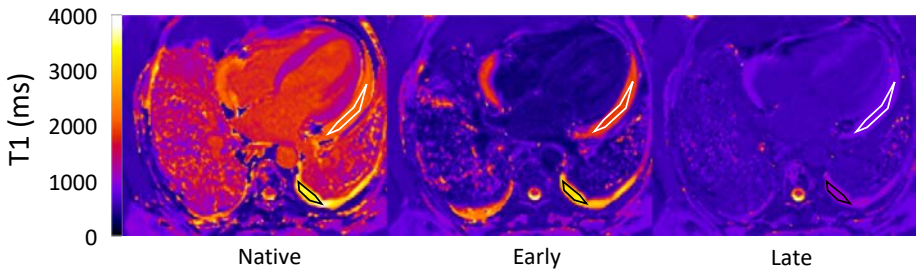

Figure 14. Example T1 maps taken in **Study I,** before, early, and late after contrast administration. The white and black regions of interest illustrate how measurements were delineated in the pericardial and pleural effusions. (Reproduced under the Creative Commons Attribution License 4.0)

In **Study II**, T1 mapping consisted of a short-axis stack encompassing the heart and the ascending aorta. It was screened for pericardial fluid visible as areas with native T1 values above 2500 ms. If perciardial fluid was present, a slice perpendicular to the short-axis slice was prescribed to enable two perpendicular measurements. T1 maps were again acquired in the same short-axis slice positions, early, (approximately 6 min) and late (25 min) after administration of an extracellular GBCA (0.05 mmol/kg, gadobutrol, Gadovist®, Bayer AB, Solna, Sweden). Example T1 maps are shown **Figure 15**.

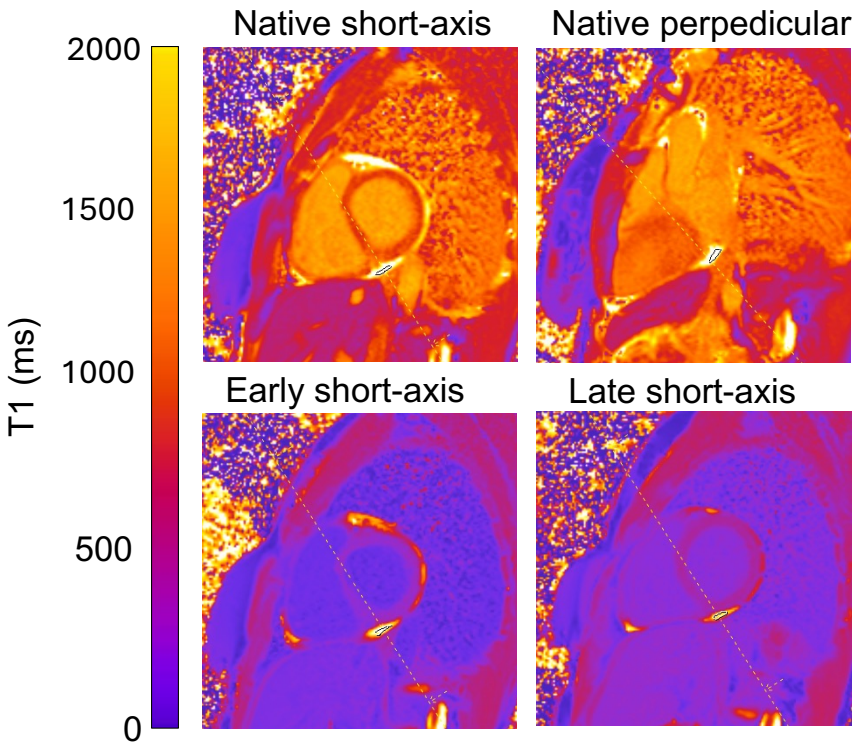

Figure 15. An example of native T1 maps from **Study II**, taken in short-axis orientation before contrast administration (top-left) and perpendicular (top-right) slice orientation. As well as early short-axis orientation (bottom-left) and late short-axis orientation (bottom-right). (Reproduced under the Creative Commons Attribution License 4.0)

Unfortunately, the use of different contrast agents in **Study I** and **Study II** means that a direct comparison of contrast dynamics in patients and healthy volunteers was not possible. The decision was made not to include normal values for GBCA contrast excretion in the final manuscript of **Study II.** It is included in the thesis for completeness and because it signifies an important learning point in the authors doctoral research education.

3.5 T1 Mapping Image Analysis

Image analysis in **Study I** was performed based on the manual delineation of regions of interest (ROI) in effusions using clinical workstations (IDS7, Sectra, Sweden). T1 values within the ROI, and its size were recorded. A criterium of 5 mm of effusion was chosen regarding whether it was possible to reliably

measure T1 values from the respective effusion. The ROI size or size of effusion in mm, required to reliably measure the T1 values of pericardial or pleural effusions is an open question. 5 mm was chosen for purposes of consistency based on clinical judgment.

Image analysis in **Study II** was performed on clinical workstations using clinical imaging software (syngo.via VB30A; Siemens Healthcare GmbH, Erlangen, Germany). ROIs were manually prescribed in the same volume of pericardial fluid of both the short axis and perpendicular slices. A 3D cursor feature was used to ensure measurement in the -me volume of pericardial fluid in both slice orientations. The anatomical location of the pericardial fluid, standard deviation (SD) of T1 values within the ROI, and its size were recorded. The following criteria were used to define a reliable measurement:

I. The ROI size needed to be >10 mm^2 and <50 mm^2.

II. The coefficient of variation of measured values within the ROI needed to be <10%.

III. The relative difference in measured values between the short axis and perpendicular slice orientations needed to be below 5%.

The coefficient of variation was defined as the ratio of the SD to the mean within in each ROI. The relative difference in native T1 between short axis (SA) and perpendicular (P) measurements was defined as:

$$\text{relative difference} = \text{short axis} - \text{perpendicular} \Big/ \frac{\text{short axis} + \text{perpendicular}}{2} \quad (3\text{-}1)$$

This was done to attempt to standardize and increase the reliability of the measurements. These were again arbitrarily chosen as there is no objective threshold to inform the size, coefficient of variation, or relative difference needed for a reliable measurement.

In both **Studies I and II,** analyzed variables in the respective effusions and normal pericardial fluid were native T1, the difference between T1 native and T1 acquired early (ΔT1 early) and late (ΔT1 late) after contrast injection, the change in R1 values (ΔR1 early and ΔR1 late) and the effusion-volume-independent early-to-late contrast concentration ratio (ΔR1 early/ΔR1 late), where ΔR1 = 1/T1 post-

contrast - 1/T1 native. In addition, an estimation of GBCA concentration was made using the formula

$$[Gd] = \frac{\Delta R1}{r1} \tag{3-2}$$

where r1 is the specific relaxivity of each GBCA. The r1 of gadoteric acid, used **Study I**, and gadobutrol used in **Study II**, have been previously been determined to be 3.6 L/mmol^{-1}/s^{-1} and 5.2 L/mmol^{-1}/s^{-1} in plasma at 1.5 T and 37° C (94).

In addition, a phantom experiment was performed where plastic bottle containing 500 ml of sterile water was used to emulate the long T1 values of a pericardial or pleural effusion. To obtain a reference T1 value, free from heartrate dependence, the phantom was first imaged using a B1 corrected variable flip angle T1 mapping sequence. The phantom was then imaged several times using the 5(3)3 MOLLI sequence flip angle 3° and 15°, matrix size 156x256 and field of view 380 mm * 309 mm.

3.6 Real-Time Phase-Contrast Velocity Encoded Imaging

In **Study III and IV**, imaging was performed at 3T in a basal short-axis view over a 30 s acquisition during free breathing using a research sequence. In **Study IV**, each participant exited the scanner, walked in a circle around it and proceeded to be imaged again using identical parameters.

Typical image acquisition parameters included: repetition time 3.7 ms, water excitation pulse with flip angle 10°, slice thickness 8 mm, FOV 360x266 mm^2, matrix 208x135, aliasing velocity (VENC) 150 cm/s and shared velocity encoding enabled (95). Compressed sensing with an acceleration factor of 7.7 was used to achieve a temporal resolution of 48 ms (96). RT-PC velocity-encoded imaging data were acquired with through-plane velocity encoding and a slice position across the atrioventricular plane from a horizontal long-axis view in end-diastole as shown in **Figure 16**. A 30-second data set of RT-PC data was acquired per patient, spanning several cardiac and respiratory cycles. All participants were in sinus rhythm at the time of CMR imaging. Phase offset errors were corrected based on estimation in stationary background tissue (97).

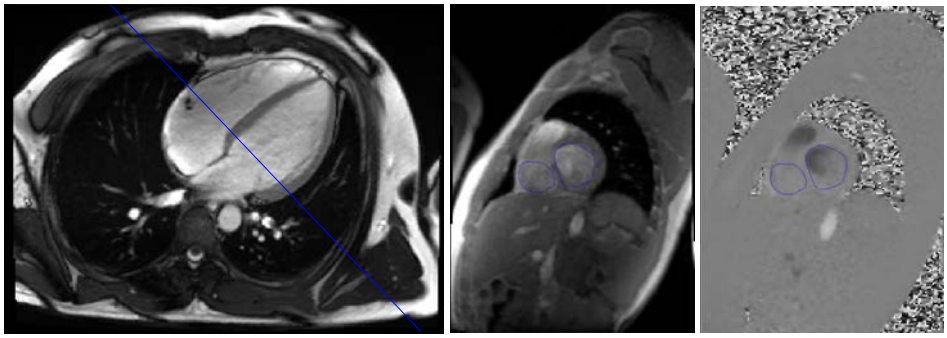

Figure 16. A four-chamber long-axis cine acquisition in end-diastole shows how the plane for through-plane RT-PC imaging was prescribed (left). Regions of interest for the mitral and tricuspid valves are shown in magnitude (middle) and phase (right) images.

3.7 Semi-Automatic Analysis of RT-PC Images

RT-PC velocity measurements and analysis were performed off-line using an in-house developed software as a plugin to the software program Segment (Medviso AB, Lund, Sweden) (98). The plugin was developed using source code available for research in the MATLAB software development environment (The MathWorks, Inc., Natick, Massachusetts, United States). The source code is freely available as a Github fork of Segment at https://github.com/SuperSimon81/segment-open-and-respiratory-variation.

The plugin was designed to allow the user to manually define ROIs encompassing the mitral and tricuspid orifices and propagate them across all time frames. The ROIs could be reviewed in each frame to ensure correct placement. The negative component of the flow velocity present in the mitral ROI during systole, part of the aortic outflow, was then used to segment the data into individual cardiac cycles by considering the peak negative flow as separating the cardiac cycles. This segmentation could be edited by the user.

Spectral plots of mitral and tricuspid velocities are displayed, and the mean of pixels with velocities higher than the 98th percentile are used to construct a velocity-time curve where the peak early filling velocities are identified and indicated. The user can increase or decrease the number of pixels used to construct the velocity-time curve, the visibility of which can be toggled, to ensure a visually acceptable fit with the spectral plot.

The peak early filling velocity is then identified within each cardiac cycle by identifying the first local maxima with a value exceeding the mean plus one standard deviation of the velocity in that timeframe. An example spectral

velocity-time plot is shown in Figure 2. The respiratory variation in early inflow velocities is then defined as the absolute value of the change as a percentage of the maximum early inflow velocity as follows

$$\text{respiratory variation} = \frac{\text{maximum velocity} - \text{minimum velocity}}{\text{maximum velocity}} \times 100 \tag{3-3}$$

Additionally, a graph with time on the horizontal axis and voxels in a vertical line selected from the magnitude image on the vertical axis is also displayed to enable visual tracking of the lung-diaphragm interface. While not strictly necessary, this allows the user to ensure that each reported peak occurred during inspiration or expiration respectively.

Additionally, a second and third definition of respiratory variation, found in the literature, was also used where Eq. (3-4 follows (99) and Eq. (3-5 and (3-6 follows (46)

$$\text{respiratory variation} = \frac{\text{expiratory velocity} - \text{inspiratory velocity}}{\text{expiratory velocity}} \times 100 \tag{3-4}$$

$$\text{mitral respiratory variation} = \frac{\text{expiratory velocity} - \text{inspiratory velocity}}{\text{inspiratory velocity}} \times 100 \tag{3-5}$$

$$\text{tricuspid respiratory variation} = \frac{\text{inspiratory velocity} - \text{expiratory velocity}}{\text{expiratory velocity}} \times 100 \tag{3-6}$$

3.8 Statistical Analysis

The normality of distributions was assessed visually, using Q-Q plots, and in ambigous cases the Shapiro-Wilk test for normality. Data was reported as median [interquartile range] or mean±SD as appropriate. Mean value comparisons were made using parametric paired or unpaired t-tests as appropriate. A p-value of less than 0.05 was considered statistically significant.

No correction of the level of significance due to multiple t-tests was performed. The coefficient of repeatability and non-parametric limits of agreement were calculated as described by Bland-Altman et al. (76,100). ICC estimates and their 95% confidence intervals were calculated using a single rating (k=1), absolute-agreement and a 2-way random-effects model (77). Mean absolute error was derived as the mean of absolute differences between the two sets of observations, divided by the mean of the observations. All statistical calculations were performed using the software package R (R Core Team 2020, Vienna, Austria).

4 Results

4.1 T1 Mapping and Contrast Dynamics

In **Study I,** native T1 values were lower in pericardial effusions (2912 [2567–3152] ms, range 1855–3744, n = 69) compared to pleural effusions (3148 [2692–3494] ms, range 1481–3938, n = 54, p = 0.005). There was no relationship between heart rate and the native T1 of pericardial effusions (R^2<0.01, p=0.35).

ΔT1 late values of pericardial effusions were (1342 [1029–1681] ms, range 602–2504), there was contrast excretion into all pericardial effusions, manifested as a sizable reduction in T1 late after contrast administration (>602 ms reduction in T1 for all). Similarly, ΔT1 late values of pleural effusions were (2210 [1768–2508] ms, range 1234–3146), there was contrast excretion into all pleural effusions, manifested as a substantial reduction in T1 late after contrast administration (>1234 ms reduction in T1 for all). The evolution of T1 values at each time point is shown in **Figure 17**.

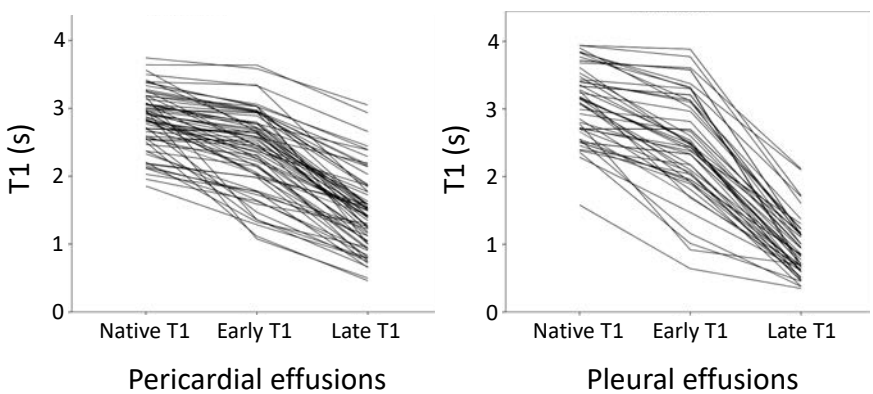

Figure 17. Line graph showing evolution of T1 values in pericardial and pleural effusions before (Native T1), early (Early T1) and late (Late T1) after GBCA injection. A straight line would indicate that contrast was not excreted. (Reproduced under the Creative Commons Attribution License 4.0)

The ΔR1 of the blood pool early after contrast agent administration was (6.8 [5.3–8.3] s^{-1}, range 1.6–15 s^{-1}), and decreased at the late time point (2.1 [1.8–2.4] s^{-1}, range 1.2–3.5 s^{-1}, $p<0.001$). The ΔR1 of the myocardium early after contrast agent administration was (3.0 [2.4–3.5] s^{-1}, range 0.1–7.7 s^{-1}), and decreased at the late time point (1.1 [0.9–1.2] s^{-1}, range 0.6–2.2 s^{-1}, $p<0.001$). ΔR1 is directly proportional to relative contrast concentration, and consequently, the blood pool and the myocardium had a relatively high contrast agent concentration early after administration, which decreased over time between the early and late time points. By comparison, both types of effusions had an increasing relative contrast agent concentration over time.

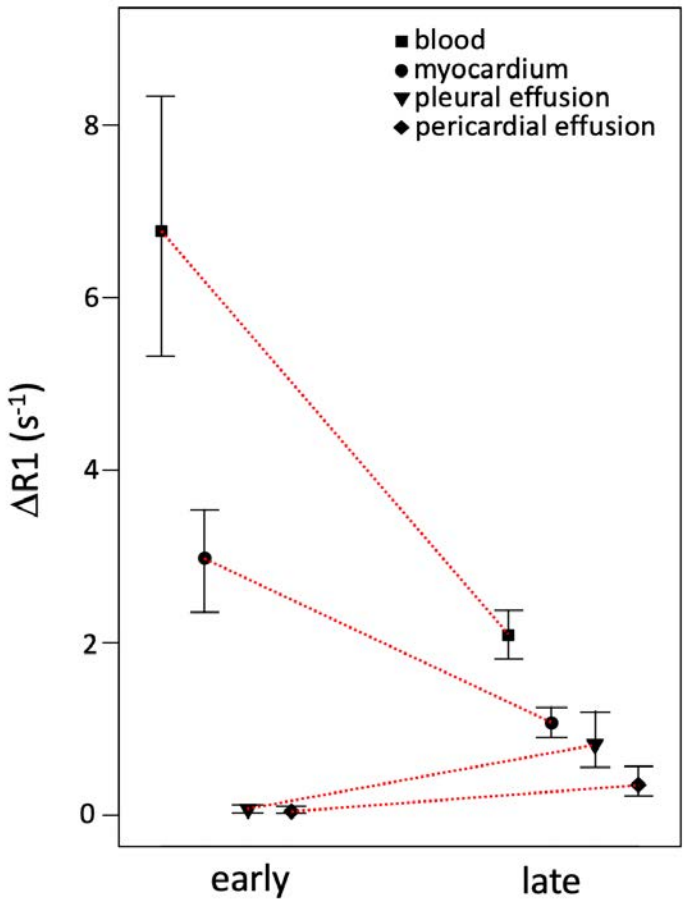

Figure 18. Plot of ΔR1 for the blood, myocardium, pleural effusion, and pericardial effusion both early and late after contrast administration. Symbols denote the median, and whiskers the interquartile range. The red lines illustrate the change in ΔR1. ΔR1 is proportional to contrast agent concentration. Note how blood and myocardium have a relatively high contrast agent concentration early after contrast administration, which then decreases over time at the late time point. By comparison, both the pleural and pericardial effusions have measurable but low relative contrast agent concentrations early after contrast administration, which increase over time at the late time point, to a level that is lower than for blood and myocardium. (Reproduced under the Creative Commons Attribution License 4.0)

The early-to-late contrast concentration ratio (ΔR1 early/ ΔR1 late) was higher in pericardial effusions (0.180 [0.0800.290], range 0.003–0.530), compared to pleural effusions (0.080 [0.003–0.144], range 0.002–0.683, $p < 0.001$), indicating that pericardial effusions have more prominent early excretion dynamics. A comparison is seen in **Figure 19**.

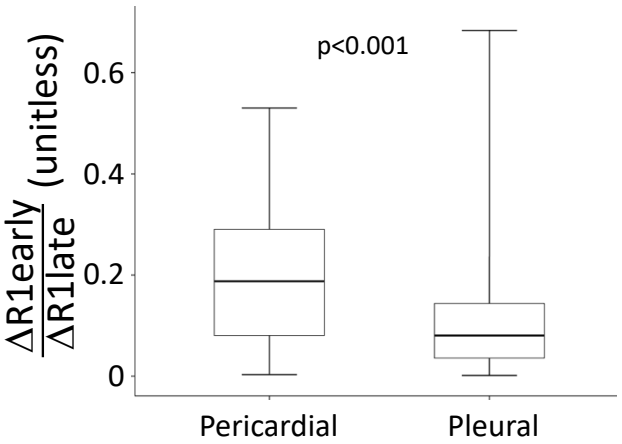

Figure 19. Boxplot of the ratio formed by ΔR1early and ΔR1late for pericardial and pleural effusions. This ratio is independent of the volume of the effusion. The boxes indicate median and interquartile range, and whiskers the full range. (Reproduced under the Creative Commons Attribution License 4.0)

Estimated GBCA concentration at the early timepoint was (12.4 [7.1–28.7] mmol/mL, range 0.1–164.8) for the pericardial effusions and (20.0 [7.9–33.8] mmol/mL, range 0.2–258.3) for the pleural effusions. Estimated GBCA (gadoteric acid) concentration at the late timepoint was (98.2 [63.3–154.7] mmol/mL, range 16.9–491.7) for the pericardial effusions and (228.5 [154.8–331.5] mmol/mL, range 55.9–645.1) for the pleural effusions.

In **Study I,** the effect of heart rate on T1 measurements of pericardial and pleural fluids was investigated using a phantom. . Electrocardiogram signals were simulated with RR-intervals ranging from 400 to 1500 ms in 100 ms increments. Measurements were obtained using a circular ROI 4 cm in diameter placed in the center of the bottle. The percentage of relaxation r immediately before the second inversion of the MOLLI sequence using the following formula:

$$r = 1 - e^{-\frac{t}{T_1^*}} \quad (4\text{-}1)$$

Where t was the time between the first and second inversion in milliseconds, i.e. 8 times the RR-interval for a MOLLI readout, and T1* the apparent relaxation time constant in milliseconds as measured by the MOLLI sequence.

The acquisition parameters of the B_1 corrected variable flip angle sequence used in the phantom study were: flip angle 3° and 15°, matrix size 156x256 field of view 380 mm * 309 mm.

The reference T1 value of the sterile water phantom was measured to 3011 ms. The results of variable RR-intervals on T1 measurements in the phantom using MOLLI are reported in Table 3. For RR-intervals below 600 ms, the MOLLI sequence failed to report T1 values, presumably due to lack of convergence of the curve fitting algorithm.

Table 3. The relationship between heart rate and T1 mapping measurements

RR (ms)	HR (bpm)	T1 (ms)	Curve fit uncertainty in SD (ms)	T1* (ms)	Relaxation (%)
600	100	3363	1000	1000	98%
700	86	2948	882	1530	96%
800	75	2853	464	1949	94%
900	67	2808	256	2198	95%
1000	60	2818	158	2389	95%
1100	55	2827	106	2498	96%
1200	50	2859	73	2604	97%
1300	46	2867	54	2612	97%
1400	43	2878	41	2645	98%
1500	40	2910	33	2674	98%

The T1 values of a phantom with a reference T1 value of 3011 ms imaged using MOLLI acquisitions with increasing heart rates (HR). The curve fit uncertainty was obtained from the SD maps provided by the MOLLI reconstruction, T1* is the apparent T1 relaxation time constant and relaxation the percentage of relaxation after 8 RR-intervals, immediately before the second inversion of the MOLLI sequence.

In **Study II,** a reliable T1 measurement was possible in 26/30 (87%) of volunteers. Four (13%) volunteers did not fulfill the reliability criteria detailed in the Methods section. Native T1 of pericardial fluid was 3262 ± 163 (95% normal limits 2943–3581 ms) and did not differ in the perpendicular slice orientation (3267 ± 173 ms, P = 0.75).

ΔR1 early was 0.11±0.05 s^{-1} and ΔR1 late 0.37±0.15 s^{-1} and the effusion-volume-independent early-to-late contrast concentration ratio ΔR1 early/ΔR1 late of 0.30±0.10.

The estimated GBCA (gadobutrol) concentration in pericardial fluid at the early time point was (20±9 mmol/mL) and at the late time point (70±28 mmol/mL).

Normal reference ranges are shown in Table 4.

Table 4. Mean and normal reference range for characteristics of pericardial fluid

	mean	95% limits
Native T1, ms	3262	2943-3581
T1 early, ms	2458	1882-3034
T1 late, ms	1552	916-2188
ΔT1 early, ms	804	245-1363
ΔT1 late, ms	1710	1036-2384
ΔR 1early, s^{-1}	0.11	0.01-0.20
ΔR1 late, s^{-1}	0.37	0.08-0.66
ΔR1 early/ΔR1 late, unitless	0.30	0.10-0.50
[Gd] early, mmol/mL	20	2-39
[Gd] late, mmol/mL	70	15-126

Early values were imaged 6 minutes after contrast injection with and late values were imaged 26 minutes after contrast injection. The GBCA used was gadobutrol and the dose used 0.05 mmol/kg.

No correlation between age, heart rate or ROI area and T1 values was found as seen in **Figure 20**.

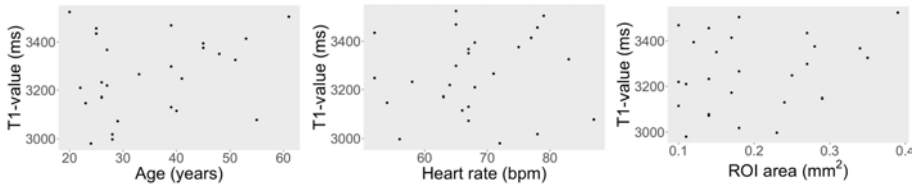

Figure 20. T1 values from pericardial fluid and subject age (left), heart rate (middle), and ROI area (right). There were no significant correlations, and hence a line of regression has been intentionally omitted.

4.2 Ventricular Interdependence

In **Study III,** the respiratory variation in mitral and tricuspid peak early inflow velocity in patients (n=24) without constrictive pericarditis or pericardial effusion was (mean±SD) 22±7% (upper normal limit 35%) and 38±7% (upper normal limit 51%). An example screenshot of a representative patient without constrictive physiology is shown in **Figure 21**.

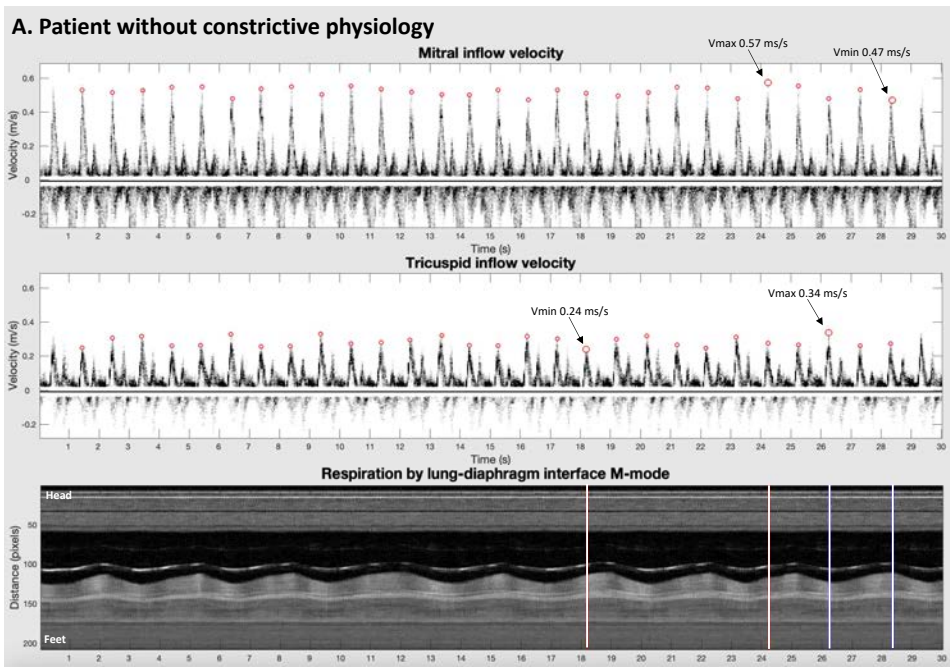

Figure 21. Screenshot of the plugin. The upper panels show spectral plots of all velocities with peak early velocities denoted as a red circle. A graph with time on the horizontal axis and voxels in a vertical line selected from the magnitude image on the vertical axis is also created. This amounts to a time-motion graph not unlike M-mode (motion mode) echocardiograph which enables visual tracking of the lung-diaphragm interface. In this graph, white lines are used to indicate each mitral and tricuspid V_{max} and V_{min} and thus allow the user to ensure that each reported peak occurred during inspiration or expiration, respectively.

The patient with constrictive pericarditis had a respiratory variation in mitral and tricuspid peak early inflow of 51% and 44% as shown in **Figure 22**.

The patient with 35 mm pericardial effusion had a respiratory variation in mitral and tricuspid peak early inflow velocities of 62% and 64%, respectively as shown in **Figure 23**.

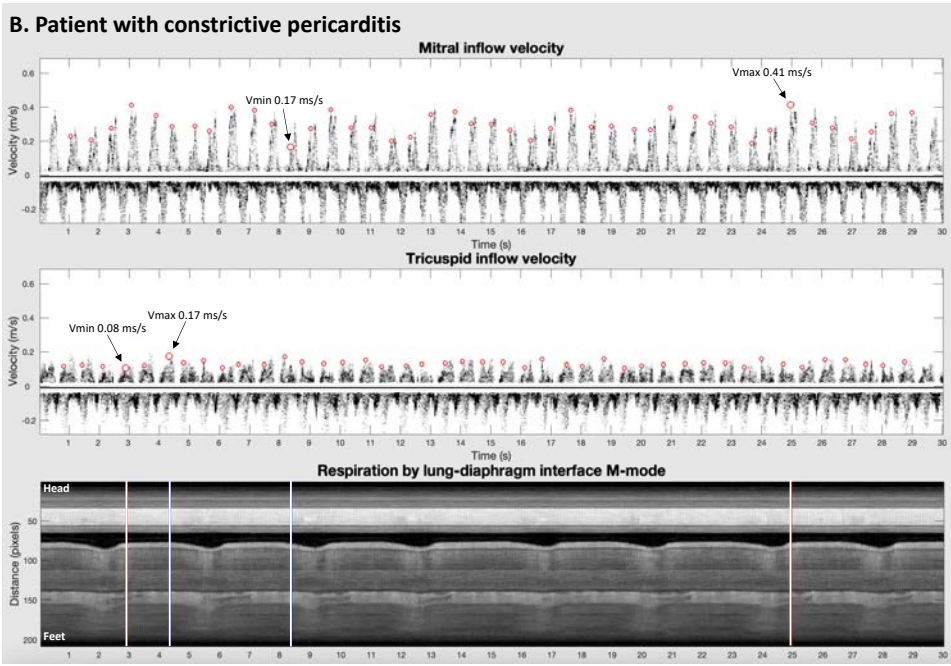

Figure 22. Screenshot showing results from a patient with constrictive pericarditis. Mitral and tricuspid variation is 51% and 44%.

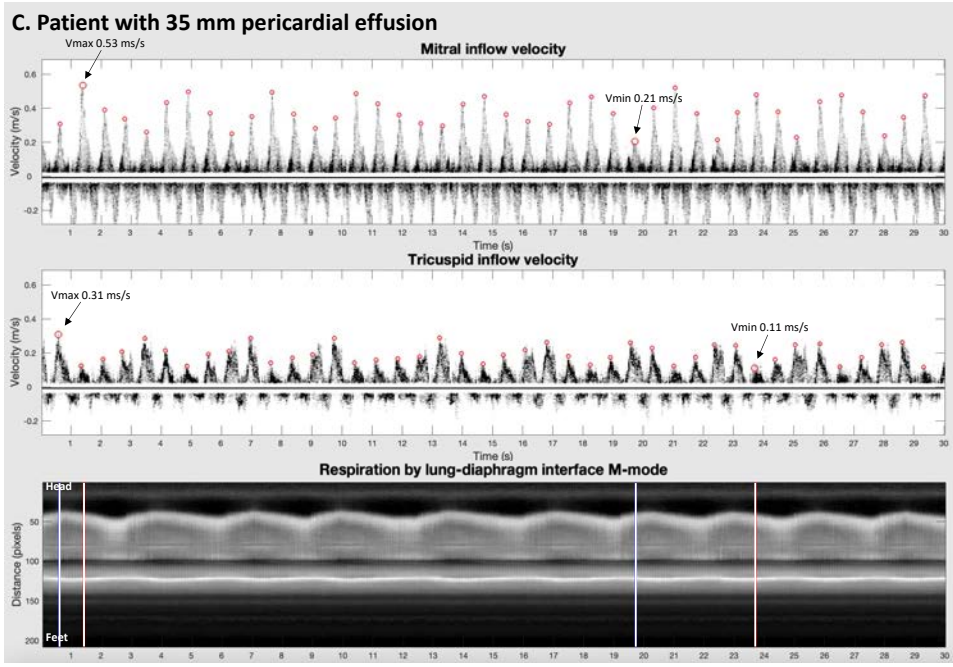

Figure 23. Screenshot showing results from a patient with 35 mm pericardial effusion. Mitral and tricuspid variation is 51% and 44%.

In **Study IV**, the test-retest repeatability results did not differ (mitral 27±7 vs. 28±5%, p=0.66 and tricuspid 47±10 vs. 47±11%, p=0.84). The coefficient of repeatability was 9.1 % and 9.8 % for mitral and tricuspid respiratory variation. For intra-observer reproducibility, the results of pooled acquisitions (n=26) did not differ (mitral 28±6 vs 28±6 %, p=0.66 and tricuspid 48±11 vs 48±11 %, p=0.84). Bias and non-parametric 95% limits of agreement were 0% (-4%-0%) and 0% (-5%-6%) for mitral and tricuspid respiratory variation. The results are summarized in **Figure 24**.

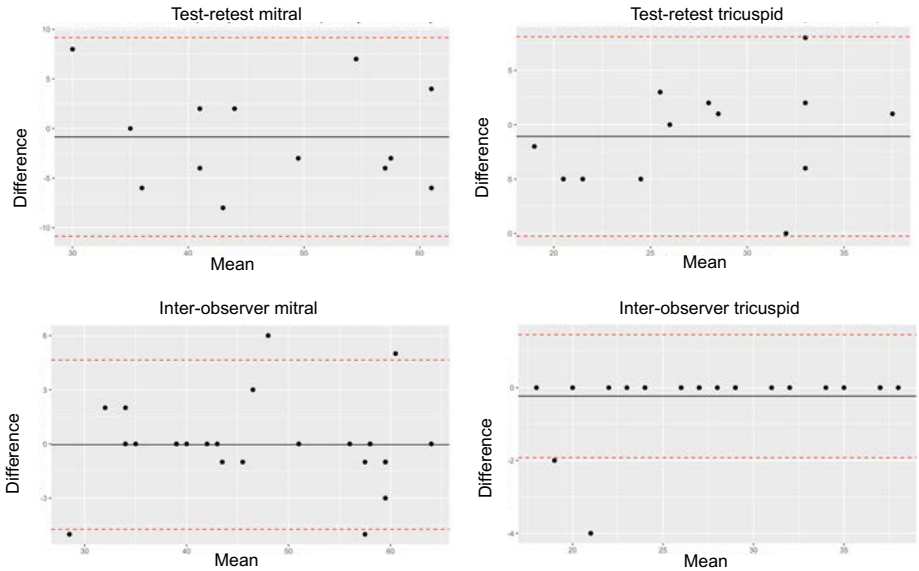

Figure 24. Bland-Altman plots of the difference between test-retest results for mitral velocity (top-left), test-retest for tricuspid velocity (top-right), inter-observer results for mitral velocity (bottom-left), and inter-observer results for tricuspid velocity.

5 Discussion

5.1 Native T1 and GBCA Contrast Dynamics

The fact that GBCA is excreted into pericardial and pleural effusion fluids is perhaps not surprising, given that GBCA used in CMR exclusively has an extracellular distribution.

Study I confirms that excretion occurs in all pericardial and pleural effusions and that there is considerable variability in both the amount and rate of excretion. Pericardial effusions were found to have a lower T1 than pleural. This is expected as pericardial effusions contain more proteins that lower T1 than pleural effusions (101). Pericardial and pleural effusions showed similar changes in early relaxation rate (ΔR1 early), but pleural effusions exhibited a greater increase in the late relaxation rate (ΔR1 late). This leads to a smaller ratio of ΔR1 early to ΔR1 late in pleural effusions, suggesting more pronounced late excretion dynamics compared to early excretion. It is important to highlight that both ΔR1 early and ΔR1 late are influenced by the volume of the effusion, while this term cancels out in the ratio formed by ΔR1 early to ΔR1 late.

One study discovered that using T1-weighted imaging to measure the excretion of GBCA into pleural effusions could perfectly distinguish between transudates and exudates, with a sensitivity and specificity of 100%. That study noted no difference in T1-weighted signal intensities in transudates following the injection of GBCA and this led to the assumption that the higher pleural permeability in exudates facilitated the excretion of these contrast agents into the effusion (102). The findings in **Study I**, using the more sensitive quantitative imaging technique T1 mapping, demonstrate that contrast excretion occurs in all types of pleural effusions. Given that it is highly unlikely that all effusions, in **Study I** were exudates, the use of contrast dynamics as a means to differentiate between transudate and exudate appears to be more complex than previously believed.

Over time, the concentration of GBCA in both the blood pool and the myocardium decreases. Except in cases of myocardium with acute microvascular obstruction, there is a quick exchange of GBCA between the myocardium and blood. This results in a dynamic equilibrium, leading to a reduction in the relative concentration of GBCA over time following an intravenous bolus, mainly due to renal clearance. Conversely, **Study I** indicates

an increase in the relative concentration of the contrast agent in both types of effusions over time after administering GBCA.

While blood has an extracellular space equal to one minus the hematocrit, serous effusions contain few cells, suggesting that it should be approximately roughly twice that of blood. In **Study I**, the contrast agent concentration in the effusions did not surpass that of the blood at later time points as seen in **Figure 18**. This suggests that the effusions do not establish a dynamic equilibrium with the blood as is required for the calculation of the extracellular volume fraction (ECV) (103). Thus, a calculation of ECV for these effusions is not consistent with the physiology of ECV and is terminologically inappropriate. This was requested by one reviewer of **Study I** but is omitted in this thesis. The observed concentration exhibited significant variation. This reflects different physiological characteristics, amount, and rate with which GBCA is distributed into the effusions.

Research using CT has demonstrated varying outcomes, with some studies indicating higher attenuation in exudates than transudates in pleural effusions, although there is an overlap in results (104–106). Contrarily, one study reported greater attenuation in transudates compared to exudates (107). Regarding the use of iodinated contrast agents in these studies, it was either infrequently used (104), not evaluated despite being administered (106), used without noting any significant differences in attenuation before and after contrast (105), or used and differences observed only in transudates (107). In the context of pericardial effusions, a CT study detected variations in attenuation before and after contrast in certain cases, and all these cases had a benign progression (108), while another study found no such differences (109). Overall, the findings regarding contrast dynamics in CT imaging have been notably inconsistent.

Contrasting these results, **Study I** used T1 mapping CMR and showed the excretion of GBCA in all examined pericardial and pleural effusions. Although CT and T1 mapping CMR employ different measurement techniques, iodinated constrast agents and extracellular GBCA share similarities in distribution and renal clearance (110,111). Furthermore, a strong correlation has been established between these two methods in the realm of quantitative tissue characterization (112).

In T1 mapping the size of the ROI can significantly impact the accuracy and reliability of the measurements. A small ROI may increase the likelihood of partial volume effects, where the signal comes from a mixture of tissues such as myocardium and fluids (blood/effusion). This leads to inaccurate T1 values. A smaller ROI means a lower signal-to-noise ratio, which makes the T1 measurements less. Achieving consistent placement of a small ROI across different time points is challenging, which can affect the reproducibility of T1 measurements.

In **Study I**, a criterium of 5 mm of effusion was chosen based on clinical judgement. There is no cut-off separating normal pericardial fluid from pericardial effusion in current echocardiography guidelines, and an effusion below 10 mm is simply categorized as mild (113).

Study II shows that T1 values can be reliably measured in the pericardial fluid of healthy volunteers. It is important to note that this is valid under the assumption that the criteria used to define a reliable measurement, described in the methods section, are adequate. The criteria include minimum and maximum ROI size criteria, within-ROI variance criteria, and between-ROI variance criteria with separately acquired and perpendicularly oriented measurements. Native T1 values of pericardial fluid in healthy volunteers were found to be similar to those in a study where T1 mapping was used in pericardial effusions presumed to be transudates. Using the native T1 threshold of 3105 ms, as suggested for exudates in that study, it can be concluded that two healthy volunteers from **Study II** exhibited lower values (114).

5.2 The Light Criteria

Aspirated *ex-vivo* effusion fluid is routinely evaluated using the Light criteria. An attractive objective for any molecular imaging attempt of effusion fluid would therefore be to do the same. Indeed, one study measured the T1 in pleural and pericardial effusions and correlated them to biochemical analysis employing the Light criteria. Good diagnostic accuracy for diagnosing transudative effusions for pleural (79% sensitivity, 89% specificity) and pericardial (sensitivity of 95%, specificity of 81%) fluid was found. Biochemical samples were available almost exclusively for exudates and the cohort was therefore supplemented with presumed transudates by including patients with pericardial and/or pleural effusions and chronic severe left ventricular systolic dysfunction (114). The validity of this approach is questionable as several studies have shown that most

pericardial effusions are misclassified as exudate by the Light criteria in biochemical analysis, and most, if not all, normal pericardial fluid is classified as exudate (18,101,115). One of the parameters of Light criteria is total fluid protein content (15). A negative correlation between protein levels and native T1 has been found in phantoms as well as *in vitro* (114) and *ex vivo* (116) effusion fluids. If biochemical testing had been available for transudates, they would presumably been classified as exudates by Light criteria, and the results would have been considerably less impressive. That is not to claim T1 mapping is useless; on the contrary, it could be argued that the results would have been more impressive if dichotomization between exudate and transudate had been done using predefined diagnostic categories and not biochemical testing with the same outcome. The classification of pericardial effusions as exudate or transudate should be restricted to predefined diagnostic categories reflecting the etiology of the effusion in the lack of biochemical testing data validated specifically for pericardial effusions.

It is important to consider that diuretics, commonly used in treating heart failure, can influence the composition of effusion fluid. They tend to increase protein concentration or, alternatively, reduce the water content in the fluid. This alteration can lead to a misclassification of the effusion as an exudate when using Light criteria (17). Given the inverse relationship between protein content and native T1 values in effusion fluids, there is a plausible risk that effusions in patients undergoing diuretic treatment might be incorrectly identified as exudates through T1 mapping techniques.

Contrast dynamics, as investigated in **Study I and II** may offer additional insights into the state and permeability of the pericardium using contrast agents routinely used during CMR imaging in accordance with current clinical guidelines (117).

In the **Study II**, we used the 5s(3s)3s version of the MOLLI technique for T1 cardiac mapping. There are several other cardiac T1 mapping methods available, such as SASHA (118), shMOLLI (119), and SAPPHIRE (120), each with its individual pros and cons. MOLLI was chosen as it is the most commonly used in clinical settings. The standard 5(3)3 MOLLI variant is known to be affected by heart rate (121). In **Study I**, there was no relationship between heart rate and native T1 in our study population, indicating that high heart rates did not contribute to systematic bias compared to low heart rates. The phantom experiment

summarized in Table 3 indicates that high heart rates resulted in a loss of precision but no systematic bias. The 5s(3s)3s version of MOLLI used in **Study II** offers improvements, albeit with some residual heart rate sensitivity (121). This sensitivity at high heart rates arises from incomplete relaxation and leftover longitudinal magnetization between inversions, resulting in lower recorded T1 values. The extent of this residual magnetization increases with both higher heart rates and T1 values. In **Study II**, native T1 values for pericardial fluid did not fluctuate with heart rate changes, as demonstrated in **Figure 20**. These findings are relevant for patients with hemodynamically significant pericardial effusion who often experience elevated heart rates. Future research with larger sample sizes may be justified to explore further the effect of heart rate on the long T1 values in pericardial fluid using different T1 mapping techniques.

5.3 Real-Time Phase Contrast Imaging

Study III demonstrates the clinical feasibility of using RT-PC to measure respiratory variations in transvalvular peak early velocities and provides normal values for these measurements.

The normal values obtained in this study are higher compared to those derived from Doppler echocardiography. A seminal research article on the respiratory changes associated with cardiac tamponade and pericardial effusion noted that there was very little respiratory variation in the peak early mitral inflow velocity in healthy individuals (38). A different study demonstrated negligible respiratory variation in the velocity-time integrals of mitral inflow in normal subjects (39). In comparison to another research that used the same RT-PC technique and equation for calculating respiratory variation (46), the findings from **Study III** show significantly higher results than those observed in the healthy control group. This discrepancy might be explained by the extended acquisition time in our study. A longer acquisition period, around 30 seconds compared to 10-20 seconds in other studies, could potentially increase the chance of recording a mitral or tricuspid peak early inflow velocity that aligns precisely with the timepoint where the hemodynamic impact of either inspiration or expiration is greatest. Notably, there are no recommendations for the duration of Doppler recording when evaluating respiratory variation in transvalvular peak early velocities (122,123). Comparing respiratory variation calculated from a recording of 10 seconds with a recording of 30 seconds could potentially be misleading.

Although patients with constrictive physiologies were excluded from the patient population of **Study III**, other confounding factors exist. Any clinical condition that increases the respiratory effort, such as asthma or chronic obstructive pulmonary disease, can cause an increased respiratory variation in transvalvular peak early inflow velocities. It is unlikely that a significant portion of the study population in **Study III**, suffered from these conditions. Care should be taken to properly characterize study populations of future studies as not only conditions considered cardiovascular can influence intrathoracic pressures.

5.4 Arithmetic Considerations to Respiratory Variation

Historically, due to patient-specific variations in early inflow velocities, respiratory variation has been quantified as a percentage. This percentage is calculated using either the positive, negative, or sometimes the absolute difference between inspiratory (Vinsp) and expiratory (Vexp) early inflow velocities as the numerator, with one of these values serving as the denominator.

For mitral velocities, selecting Vinsp as the denominator indicates an expiratory increase represented as a fraction of Vinsp. Conversely, using Vexp as the denominator implies an inspiratory decrease as a fraction of Vexp. In the context of tricuspid velocities, this relationship is inversed. The literature, however, does not consistently specify the method of calculation, though sometimes an implicit definition can be inferred (38,40,99,123–127). Several authors conceptualize mitral respiratory variation as an inspiratory decrease and tricuspid respiratory variation as an inspiratory increase, possibly influenced by the traditional definition of pulsus paradoxus (128). Others define maximal respiratory change as either the expiratory increase or decrease in early inflow velocities (46), while some compare the change in early inflow velocity during respiratory phases against apnea (129,130). Another simply reported respiratory absolute change in peak velocities (131).

According to current guidelines from the American Society for Echocardiography, respiratory variation in both mitral and tricuspid velocities should be calculated as the difference between Vexp and Vinsp, with Vexp as the denominator (99). This approach leads to a description of mitral early inflow as a percent decrease and tricuspid early inflow as a percent increase. However, considering that a percent increase is always greater than a corresponding decrease when calculated as a percentage, it would be more consistent to describe tricuspid variation as a decrease as well, thus employing Vinsp as the

denominator. In **Study III and IV**, respiratory variation in mitral and tricuspid peak early inflow velocities was calculated as the absolute change in velocity divided by the maximum velocity.

5.5 Methodological Considerations In Respiratory Variation

When recording respiratory variation in mitral peak early inflow velocities using Doppler echocardiography, a cursor is placed at the mitral leaflet tips and all ultrasound echoes from that 3-dimensional volume are recorded and usually plotted over time in a velocity-time curve.

In through-plane phase contrast CMR, a ROI is drawn around the mitral orifice, and all pixels inside the ROI are considered and plotted against time. The pixel to be chosen to generate the velocity-time curve in this case is not a trivial problem. It is possible to make a spectral plot where each pixel present in the ROI at each time point contributes to the intensity at a certain level of velocity. The result is quite similar to a Doppler velocity-time curve which is attractive in this use case. It was found that in generating the quantitative velocity-time curve used for the determination of the peak velocity, instead of using the maximum velocity in each timeframe, using the 98th percentile of all velocities could reduce the noisiness of the signal, which would otherwise be jagged and rough in appearance.

Many other methods were considered but abandoned. The velocity-time curve was generated from one, four, or nine pixels in a square shape with the highest velocity in the entire recording. The square shape was allowed to move between timeframes, moving towards a higher velocity with various constraints. Once all peak inflow velocities are found, the respiratory variation can be determined. This problem is also non-trivial. Should only one respiratory cycle be considered, many respiratory cycles averaged, and if so how many, or the maximum and minimum velocities within a certain predetermined time used for the calculation, and if so during what amount of time. In **Study III and IV**, simplicity was chosen, and the entire 30-second recording was considered. The correct methodology will ultimately be found when evaluated in clinical patients with constrictive pericarditis or hemodynamically significant pericardial effusion.

5.6 Repeatability and reproducibility

Study IV, assessed the test-retest repeatability and inter-observer reproducibility of ventricular interdependence, quantified as respiratory variation in mitral and tricuspid early filling velocities using RT-PC CMR. Notably, there are no existing studies on test-retest or inter-observer reproducibility for ventricular interdependence using any metrics, whether through invasive pressure measurements, pulsed wave Doppler echocardiography, or phase-contrast CMR.

The most relevant comparisons to **Study IV** are studies on echocardiographic Doppler measurements of diastolic function. The few available studies concern intra- and inter-observer reproducibility rather than test-retest repeatability (19, 20). One study did investigate test-retest repeatability, but it used diagnostic algorithms rather than specific measures like early inflow velocity (21). Another relevant study examined the test-retest repeatability of diastolic function parameters, including the ratio of mitral peak early and atrial inflow velocities (E/A-ratio) (22). This measure can offer a comparison to our study, as both involve assessing two peak velocities. However, it must be emphasized that these two measures are not identical as it can be more challenging to measure the peak atrial inflow velocity compared to the peak early inflow. The E/A-ratio is further measured during breath-hold in contrast to respiratory variation during free breathing in **Study IV**. The authors reported a strong ICC of 0.94 for the E/A-ratio at the mitral leaflets, and a slightly lower ICC of 0.76 at the annular level, which aligns with our findings. Another study indicated a mean absolute error of 22% for the E/A-ratio, compared to our 13% and 7% for mitral and tricuspid respiratory variation (23). A separate study on phase contrast CMR of relevance reported good to excellent test-retest repeatability for cardiac blood flow, specifically right ventricular systolic outflow (24).

The test-retest repeatability is much greater than the inter-observer reproducibility in **Study IV**. This is also the case in the study that estimated both in the setting of diastolic function and echocardiography (22). For CMR and echocardiography, performing data collection in the same conditions but at two different time points, assuming the physiology is unchanged, will likely cause more variability than two different observers analyzing the same collected data. This will likely hold for any quantitative technique. It is, therefore, quite surprising that test-retest repeatability studies are lacking in favor of inter-observer reproducibility studies. This is likely because performing data analysis twice is usually easier and more convenient than collecting the data twice.

The excellent inter-observer reproducibility in **Study IV** is likely due to the semi-automatic nature of the software tool. An inappropriately delineated ROI of the mitral or tricuspid orifice will result in a spectral plot and velocity-time curve that will provide correct peak velocities as long as one tricuspid ROI does not overlap the mitral or include noisy signals from outside the myocardium. As such the geometry of the ROI does not have to be as precise as in, for example, segmentation of the left ventricle. If one, four, or nine connected pixels in the ROI were chosen by the user or by other means to construct the velocity-time curve, the inter-observer reproducibility would likely be worse.

6 Conclusions

Based on results from all studies, the main overall conclusion of this thesis is that CMR has the potential to become a useful tool in the evaluation of pericardial effusion and constrictive pericarditis. Both molecular imaging evaluation of effusive fluids and hemodynamic evaluation of ventricular interdependence is feasible using CMR. The technical prerequisites, T1 mapping, and phase contrast sequences are available on most commercial clinical MRI scanners, and the software needed is open-source.

The conclusion of **Study I** is that intravenous extracellular GBCA is excreted into both pericardial and pleural effusions in all patients. Compared to pleural effusions, pericardial effusions had a lower native T1, consistent with lower relative fluid content in relation to other components such as proteins and more prominent early excretion dynamics.

The conclusion of **Study II** is that T1 can be reliably measured at 1.5 T in a normal volume of pericardial fluid in healthy volunteers, and normal reference values are presented.

The conclusion of **Study III** is that semi-automatic analysis of magnetic resonance RT-PC flow measurement is feasible and can be used to evaluate diastolic ventricular interdependence by measuring the respiratory variation in mitral and tricuspid early inflow velocities. Normal reference values are presented.

The conclusion of **Study IV** is that the proposed method developed in **Study III** to measure ventricular interdependence by quantifying respiratory variation in mitral and tricuspid peak early inflow velocity has an acceptable test-retest reliability. The inter-observer reproducibility is excellent for both.

7 Points of perspective

The clinical implications of this thesis are not immediately obvious. The benefit of placing a patient with a life-threatening medical condition, pericardial effusion, in an MRI scanner is not immediately clear. It is advisable to get a quick cursory point-of-care echocardiogram. However, a pericardial effusion is a common secondary finding in CMR scans. In one study it was found that 0.8% of persons undergoing CMR scans had a secondary finding of a pericardial effusion that was clinically significant. Being able to immediately provide some additional information as to the etiology of the effusion, perhaps transudate or exudate and the hemodynamic significance of the effusion is desirable. This thesis has not provided definite means to do this, but it has set the groundwork for future studies that hopefully will. Patients are often referred to the CMR lab with the question of constrictive pericarditis, but an assessment of ventricular interdependence using RT-PC is rarely performed. This thesis has shown that a simple, semi-automatic analysis of RT-PC images is feasible and could be included in the workup of constrictive pericarditis with ease. There is still much to be done, only one study has shown that T1 mapping can be used to separate transudates from exudate pericardial effusions (114). Results that need to be replicated. Phase contrast imaging, although an old technique, is still evolving. Increasing the temporal resolution of the signal is key in correctly characterizing the changing velocities in the blood flow.

Examples of venues and questions for future research:

I. Does contrast dynamics have any diagnostic value?
II. How does diuretic treatment change the T1 value of effusion fluid?
III. Is native T1 mapping inferior to the Light criteria?
IV. How well does the respiratory variation in transvalvular velocity measured using RT-PC determine the hemodynamic significance of a pericardial effusion compared to Doppler echocardiography?
V. How should the imaging plane be prescribed in phase contrast imaging to be as repeatable and reproducible as possible?
VI. How confounding are asthma and chronic obstructive pulmonary disease to measurements of ventricular interdependence using respiratory variation?
VII. Does decompensated heart failure affect the respiratory variation due to increased respiratory effort?

VIII. How does RT-PC compare to Doppler echocardiography as a technique to characterize diastolic filling?
IX. Is it possible to calculate the respiratory variation inline on the scanner?
X. How short must the TR and TE in phase contrast imaging be to match the performance of Doppler echocardiography?
XI. How fast can we go? What is the smallest temporal resolution possible?
XII. What is the most repeatable and reproducible way to construct the velocity-time curve?
XIII. Is in-plane better than through-plane velocity encoding to measure respiratory variation in transvalvular peak inflow velocities
XIV. Is it possible to make a respiratory resolved free breathing phase contrast pulse sequence specifically to measure respiratory variation in transvalvular peak inflow velocities?
XV. Is it possible to use real-time imaging to derive other measurements of ventricular interdependence that are better than respiratory variation?
XVI. Is an m-mode line on the septum useful?
XVII. Can right atrial strain be used?
XVIII. Can T1rho be used to characterize effusion fluid?
XIX. Can T2 mapping be used to characterize effusion fluid?

8 Catharsis

Catharsis, traditionally associated with the emotional release and purification in the realms of art and psychology, here serves as a metaphor for the agony inherent in the scientific process. This section will provide a candid examination of the various challenges, missteps, and lessons learned throughout the course of this research. It aims to shed light on the realities of scientific inquiry, an inherently iterative process where hindsight often reveals missed opportunities and alternative paths. By critically analyzing what went wrong and contemplating how different choices could have led to varied outcomes, this introspection aims not only to inform future research endeavors but also to provide a personal therapeutic acknowledgment of the imperfections present in this thesis.

8.1 Underestimating the Time Required and Difficulty of a Task

Study IV of this thesis was originally planned to be a trial by fire of the method developed in **Study III**. The general goal was to recruit patients with

hemodynamically significant pericardial effusion determined by Doppler echocardiography and perform a short CMR exam, including through-plane RT-PC, measure the respiratory variation by both methods and compare. It turns out to be problematic recruiting unstable patients to undergo CMR in a clinical setting. The first naïve approach was to discuss the study with the clinicians on the floor and arrange for them to inform the author if a patient that could be included was available. This failed as the situation for the clinicians on the floor turned out to be stressful and hectic and required their utmost attention. There is no bitterness in this realization but rather a pride in the knowledge that the patient is ultimately what matters to us, physicians. The patient had often left the Unit of Clinical Physiology if and when the author was informed of their existence, visiting the ward and finding the responsible physician, making sure everyone was satisfied with the level of patient monitoring available in the CMR lab, informing the patient about the study, allowing them time to digest the patient information, have lunch, go to the bathroom, have the nurse disconnect the intravenous catheter, assuring access to the scanner in between clinical patients, transporting the patient from the ward to the scanner and performing the scan proved to be quite time-consuming. As the author was a physician at the time, one solution was to screen all echocardiography referrals for pericardial effusion. The key would have been to talk to the technicians performing the echo to be informed at the exact moment the effusion was discovered. Unfortunately, the time is up. This study is currently up for adoption upon reasonable request to the author.

8.2 Failure to Collaborate

The original idea was for **Study II** to be a correlation study between the results of biochemical analysis of pleural and pericardial effusions and T1 mapping. An ethical application was written but not submitted, and meetings were had with persons from various departments to create the infrastructure needed for the study. An enthusiastic person was interested in collaborating. However, prior engagements, i.e., medical school and a part-time job, meant the author had to focus his attention elsewhere. Excited and ready to go the author resumed the project. It turns out the enthusiastic person has now quit. A short discussion later, it was clear that the requirements desired by the department were quite possibly deliberately designed to be so Kafkaesque so the project would never be able to proceed. It was surmised that there was no real interest in the study

and the project was abandoned. This study is also available for adoption upon reasonable request to the author.

8.3 You Cannot Pop a Burned Popcorn

In **Study I**, two readers performed segmentation in the T1 maps of pericardial and pleural effusion fluids. The split was strictly 50-50, and there was no overlap. A subset could easily have been analyzed by both and inter-observer reproducibility derived. The same argument holds for **Study II**.

When designing **Study II**, it was not realized by the author that the contrast agent used in **Study I**, had been superseded by a new one. This made comparing contrast dynamics between patients and healthy volunteers problematic and meant that only a subset of results were published.

In **Study II**, for technical reasons, the timing of the early imaging post-contrast also differed considerably between the patients and healthy volunteers, which could have easily been addressed beforehand. This meant the precious effusion-volume-independent early-to-late contrast concentration ratio (ΔR1 early/ΔR1 late) could not be compared between the patients and healthy volunteers.

In **Study IV**, it was realized after data analysis, that to be free of confirmation bias, a predetermined clinically acceptable level of disagreement between two measurements of respiratory variation should have been set.

8.4 Sometimes Grit is not Enough

My involvement in the Karolinska CMR group started as a summer project devoted to applying the principles of the parametric diastolic filling formalism (132) to RT-PC images. The idea was to design software to fit the velocity-time curve of mitral diastolic filling to an equation modeling the filling as a dampened harmonic oscillator. You had me at curve fit! It was a great learning experience and a great introduction to CMR. The hours spent trying to squeeze out the maximum temporal resolution from the RT-PC pulse sequence and simultaneously trying to find the optimal way to construct the velocity-time curve from the time-varying pixel intensities in the segmented mitral orifice cannot be understated. It just does not work, yet.

9 Acknowledgments

Thank you, Martin Ugander for believing in me and accompanying me on this journey that has been filled with the notes of both angel trumpets and devil bassoons. I would also like to point out that the question "If you would set your own deadline for this, what would it be?" is a sword that cuts both ways. I now recommend it to all my friends.

My co-supervisor, Peder Sörensson, whose clinical perspective and wisdom have gently grounded me on several occasions. You are also my greatest teacher in the clinical evaluation of CMR scans.

My co-supervisor Andreas Sigfridsson whose calm intellect taught me the basic principles of magnetic resonance in the beginning.

Henrik Engblom and Marcus Carlsson, you have both been more influential than you know.

Alexander Fyrdahl is the person who in my view personifies magnetic resonance imaging the most of any person I have ever met. Always ready to sit down and eagerly explain the technical specifics of whatever confused me at the time. The four minutes I held my breath in the scanner while listening to Iron Maidens "Run to the hills" is also a highlight.

Eltjo Haselhoff once drew me a picture and explained k-space on a transatlantic flight. It is not often one remembers the moment of realization of an abstract subject.

The practical knowledge and many clinical subtleties I have learned from Elina Malkeshi have been invaluable and I look forward to many hours of great fun while collaborating with Jenny Castaings.

Fellow PhD students Goran Abdula, Maran Maanja, Fredrika Fröjdh, Jannike Nickander, Björn Wieslander, Daniel Loewenstein, Johan von Scheele, Rebecka Johansson, Joao Ramos, Magnus Lundin, Martin Sundqvist, Karen Holst and Mona Ahmed.

Once I stopped feeling inadequate by the accomplishments of David Marlevi, I realized that this was the beginning of a beautiful friendship on many levels.

Felicia Seeman is a great role model and fellow diastologist.

Kim Roose taught me a lot about coding

I would like to thank all my wonderful colleagues at the Unit of Clinical Physiology. Alexander Bulgak, Thomas Alsérius, Jonas Jenner, Maria Eriksson, Lena Forsberg, Jakub Zajak, Anna Damlin, Daniel Ceken, Maciej Olszowka, Patrik Sundblad, Marcus Souraniemi, Christos Ntouloulis Anette Rickenlund, Pia Ullström, Kenneth Caidahl, Flemming Larsen, Marina Mijatovic and Joakim Nordenfeldt.

I would also like to acknowledge Kristoffer Lundbäck, who is a person that can always be relied upon.

Lastly, thank you to all the healthy volunteers who participated. My mother, father, sister, brother, and myself included. Volunteers for CMR research almost always have their hearts in the right place.

10 References

1. Troughton RW, Asher CR, Klein AL. Pericarditis. The Lancet. 2004;363(9410):717–27.
2. Breen JF. Imaging of the pericardium. J Thorac Imaging. 2001;16(1):47–54.
3. Imazio M, Adler Y. Management of pericardial effusion. Eur Heart J. 2013 Apr 2;34(16):1186–97.
4. Levick JR, Michel CC. Microvascular fluid exchange and the revised Starling principle. Cardiovasc Res. 2010 Jul 15;87(2):198–210.
5. Starling EH. On the Absorption of Fluids from the Connective Tissue Spaces. J Physiol. 1896 May 5;19(4):312–26.
6. Landis EM. The Relation Between Capillary Pressure and the Rate at Which Fluid Passes Through the Walls of Single Capillaries. Am J Physiol-Leg Content. 1927 Oct 1;82(2):217–38.
7. Pappenheimer JR, Soto-Rivera A. EFFECTIVE OSMOTIC PRESSURE OF THE PLASMA PROTEINS AND OTHER QUANTITIES ASSOCIATED WITH THE CAPILLARY CIRCULATION IN THE HINDLIMBS OF CATS AND DOGS. Am J Physiol-Leg Content. 1948 Feb 29;152(3):471–91.
8. Knudson JD. Diseases of the pericardium. Congenit Heart Dis. 2011 Oct;6(5):504–13.
9. Spodick DH. Acute cardiac tamponade. N Engl J Med. 2003;349(7):684–90.
10. Peebles CR, Shambrook JS, Harden SP. Pericardial disease—anatomy and function. Br J Radiol. 2011 Dec;84(Spec Iss 3):S324–37.

11. Dudzinski DM, Mak GS, Hung JW. Pericardial Diseases. Curr Probl Cardiol. 2012 Mar;37(3):75–118.

12. Imazio M, Mayosi BM, Brucato A, Markel G, Trinchero R, Spodick DH, et al. Triage and management of pericardial effusion: J Cardiovasc Med. 2010 Dec;11(12):928–35.

13. Sagristà-Sauleda J, Mercé J, Permanyer-Miralda G, Soler-Soler J. Clinical clues to the causes of large pericardial effusions. Am J Med. 2000;109(2):95–101.

14. Light RW, Macgregor MI, Luchsinger PC, Ball WC. Pleural effusions: the diagnostic separation of transudates and exudates. Ann Intern Med. 1972 Oct;77(4):507–13.

15. Light RW. The Light Criteria. Clin Chest Med. 2013 Mar;34(1):21–6.

16. Porcel JM, Vives M. Classic, abbreviated, and modified Light's criteria: the end of the story? Chest. 1999 Dec;116(6):1833–6.

17. Romero-Candeira S, Fernández C, Martín C, Sánchez-Paya J, Hernández L. Influence of diuretics on the concentration of proteins and other components of pleural transudates in patients with heart failure. Am J Med. 2001 Jun 15;110(9):681–6.

18. Imazio M, Biondo A, Ricci D, Boffini M, Pivetta E, Brucato A, et al. Contemporary biochemical analysis of normal pericardial fluid. Heart. 2020 Apr;106(7):541–4.

19. Akyuz S, Arugaslan E, Zengin A, Onuk T, Ceylan US, Yaylak B, et al. Differentiation between Transudate and Exudate in Pericardial Effusion has almost no Diagnostic Value in Contemporary Medicine. Clin Lab. 2015;61(8):957–63.

20. Shabetai R. Pericardial effusion: haemodynamic spectrum. Heart. 2004 Mar 1;90(3):255–6.

21. Sagristà-Sauleda J, Angel J, Permanyer-Miralda G, Soler-Soler J. Long-term follow-up of idiopathic chronic pericardial effusion. N Engl J Med. 1999;341(27):2054–9.

22. Guntheroth WG. Sensitivity and Specificity of Echocardiographic Evidence of Tamponade: Implications for Ventricular Interdependence and Pulsus Paradoxus. Pediatr Cardiol. 2007 Oct;28(5):358–62.

23. Gillam LD, Guyer DE, Gibson TC, King ME, Marshall JE, Weyman AE. Hydrodynamic compression of the right atrium: a new echocardiographic sign of cardiac tamponade. Circulation. 1983 Aug;68(2):294–301.

24. Reydel B, Spodick DH. Frequency and significance of chamber collapses during cardiac tamponade. Am Heart J. 1990 May;119(5):1160–3.

25. Mercé J, Sagristà-Sauleda J, Permanyer-Miralda G, Soler-Soler J. Should pericardial drainage be performed routinely in patients who have a large pericardial effusion without tamponade? Am J Med. 1998 Aug;105(2):106–9.

26. Imazio M, Adler Y. Management of pericardial effusion. Eur Heart J. 2013 Apr 2;34(16):1186–97.

27. Bergman M, Vitrai J, Salman H. Constrictive pericarditis: A reminder of a not so rare disease. Eur J Intern Med. 2006 Nov;17(7):457–64.

28. Kosmopoulos M, Liatsou E, Theochari C, Stavropoulos A, Chatzopoulou D, Mylonas KS, et al. Updates on the Global Prevalence and Etiology of Constrictive Pericarditis: A Systematic Review. Cardiol Rev. 2023 Mar 8;

29. Kontzias A, Barkhodari A, Yao Q. Pericarditis in Systemic Rheumatologic Diseases. Curr Cardiol Rep. 2020 Sep 10;22(11):142.

30. Welch TD, Oh JK. Constrictive Pericarditis: Old Disease, New Approaches. Curr Cardiol Rep. 2015 Apr;17(4).

31. Imazio M. Cardiac Catheterization and Interventional Techniques. In: Imazio M, editor. Myopericardial Diseases: Diagnosis and Management. Cham: Springer International Publishing; 2016. p. 39–45.

32. Talreja DR, Edwards WD, Danielson GK, Schaff HV, Tajik AJ, Tazelaar HD, et al. Constrictive Pericarditis in 26 Patients With Histologically Normal Pericardial Thickness. Circulation. 2003 Oct 14;108(15):1852–7.

33. Bolen MA, Rajiah P, Kusunose K, Collier P, Klein A, Popovic ZB, et al. Cardiac MR imaging in constrictive pericarditis: multiparametric assessment in patients with surgically proven constriction. Int J Cardiovasc IMAGING. 2015 Apr;31(4):859–66.

34. Pericardectomy for chronic constrictive pericarditis: risks andoutcome. Eur J Cardiothorac Surg. 1994 Sep 1;8(9):487–92.

35. Khandaker MH, Espinosa RE, Nishimura RA, Sinak LJ, Hayes SN, Melduni RM, et al. Pericardial disease: diagnosis and management. Mayo Clin Proc. 2010 Jun;85(6):572–93.

36. Dornhorst AC, Howard P, Leathart GL. Pulsus paradoxus. Lancet Lond Engl. 1952 Apr 12;1(6711):746–8.

37. Shabetai R. The effects of pericardial effusion on respiratory variations in hemodynamics and ventricular function. J Am Coll Cardiol. 1991;17(1):249–50.

38. Appleton CP, Hatle LK, Popp RL. Cardiac tamponade and pericardial effusion: respiratory variation in transvalvular flow velocities studied by Doppler echocardiography. J Am Coll Cardiol. 1988;11(5):1020–30.

39. Leeman DE, Levine MJ, Come PC. Doppler echocardiography in cardiac tamponade: exaggerated respiratory variation in transvalvular blood flow velocity integrals. J Am Coll Cardiol. 1988;11(3):572–8.

40. Simeonidou E, Hamouratidis N, Tzimas K, Tsounos J, Roussis S. Respiratory variation in mitral flow velocity in pericardial effusion and cardiac tamponade. Angiology. 1994;45(3):213–8.

41. Shaver JA, Reddy PS, Curtiss EI, Ziady GM, Reddy SC. Noninvasive/invasive correlates of exaggerated ventricular interdependence in cardiac tamponade. J Cardiol. 2001;37 Suppl 1:71–6.

42. Gonzalez MS, Basnight MA, Appleton CP. Experimental pericardial effusion: relation of abnormal respiratory variation in mitral flow velocity to hemodynamics and diastolic right heart collapse. J Am Coll Cardiol. 1991;17(1):239–48.

43. Wayne VS, Bishop RL, Spodick DH. Dynamic effects of pericardial effusion without tamponade. Respiratory responses in the absence of pulsus paradoxus. Br Heart J. 1984 Feb;51(2):202–4.

44. Spodick DH, Paladino DM. Exaggerated respiratory variation in left ventricular ejection time during lax pericardial effusion. Cardiology. 1983;70(1):1–5.

45. Spodick DH, Paladino D, Flessas AP. Respiratory effects on systolic time intervals during pericardial effusion. Am J Cardiol. 1983 Mar 15;51(6):1033–5.

46. Thavendiranathan P, Verhaert D, Walls MC, Bender JA, Rajagopalan S, Chung YC, et al. Simultaneous Right and Left Heart Real-Time, Free-Breathing CMR Flow Quantification Identifies Constrictive Physiology. JACC Cardiovasc Imaging. 2012 Jan;5(1):15–24.

47. Aquaro GD, Barison A, Cagnolo A, Todiere G, Lombardi M, Emdin M. Role of tissue characterization by Cardiac Magnetic Resonance in the diagnosis of constrictive pericarditis. Int J Cardiovasc Imaging. 2015 Jun;31(5):1021–31.

48. Reddy PS, Curtiss EI, Uretsky BF. Spectrum of hemodynamic changes in cardiac tamponade. Am J Cardiol. 1990 Dec 15;66(20):1487–91.

49. Shabetai R, Fowler NO, Guntheroth WG. The hemodynamics of cardiac tamponade and constrictive pericarditis. Am J Cardiol. 1970;26(5):480–9.

50. Goldstein JA. Cardiac tamponade, constrictive pericarditis, and restrictive cardiomyopathy. Curr Probl Cardiol. 2004 Sep;29(9):503–67.

51. Rabi II, Zacharias JR, Millman S, Kusch P. A New Method of Measuring Nuclear Magnetic Moment. Phys Rev. 1938 Feb 15;53(4):318–318.

52. Bloch F. Nuclear Induction. Phys Rev. 1946 Oct 1;70(7–8):460–74.

53. Damadian R. Tumor detection by nuclear magnetic resonance. Science. 1971 Mar 19;171(3976):1151–3.

54. Lauterbur PC. Image Formation by Induced Local Interactions: Examples Employing Nuclear Magnetic Resonance. Nature. 1973 Mar;242(5394):190–1.

55. Feynman RP, Vernon FL, Hellwarth RW. Geometrical Representation of the Schrödinger Equation for Solving Maser Problems. J Appl Phys. 1957 Jan;28(1):49–52.

56. Hanson LG. Is quantum mechanics necessary for understanding magnetic resonance? Concepts Magn Reson Part A. 2008;32A(5):329–40.

57. Feynman RP, Leighton RB, Sands ML, Feynman RP. Mainly mechanics, radiation, and heat. Nachdr. Reading/Mass.: Addison-Wesley; 2007. (The Feynman lectures on physics / Richard P. Feynman; Robert B. Leighton; Matthew Sands).

58. Taylor AJ, Salerno M, Dharmakumar R, Jerosch-Herold M. T1 Mapping. JACC Cardiovasc Imaging. 2016 Jan;9(1):67–81.

59. Salerno M, Kramer CM. Advances in Parametric Mapping With CMR Imaging. JACC Cardiovasc Imaging. 2013 Jul 1;6(7):806–22.

60. Kellman P, Wilson JR, Xue H, Ugander M, Arai AE. Extracellular volume fraction mapping in the myocardium, part 1: evaluation of an automated method. J Cardiovasc Magn Reson. 2012;14(1):63.

61. Beckett KR, Moriarity AK, Langer JM. Safe Use of Contrast Media: What the Radiologist Needs to Know. RadioGraphics. 2015 Oct;35(6):1738–50.

62. Barry WF, Forbis SE. Vicarious excretion of intravascular contrast material. J Urol. 1968;100(5):704.

63. Becker JA, Gregoire A, Berdon W, Schwartz D. Vicarious excretion of urographic media. Radiology. 1968;90(2):243–8.

64. Lautin EM, Friedman AC. VIcarious excretion of contrast media. JAMA. 1982 Mar 19;247(11):1608–10.

65. Holloway H, Nance EP, Burks D, Winfield AC. Vicarious excretion of contrast medium in patients without azotemia. Urology. 1985 Feb;25(2):201–3.

66. Hopper KD, Weingast G, Rudikoff J, Thickman D. Vicarious excretion of water-soluble contrast media into the gallbladder in patients with normal serum creatinine. Invest Radiol. 1988 Aug;23(8):604–8.

67. Arai K, Makino H, Morioka T, Yagi H, Minabe K, Takeyama S, et al. Enhancement of ascites on MRI following intravenous administration of Gd-DTPA. J Comput Assist Tomogr. 1993 Aug;17(4):617–22.

68. Hammerman AM, Oberle PA, Susman N. Opacification of ascitic fluid on delayed contrast computed tomography scans. Clin Imaging. 1990 Aug;14(3):221–4.

69. Moon MH, Goo JM, Seo JB, Song JW, Im JG. Delayed Enhancement of Pleural Effusion Following Angiography: A Case Report. J Korean Radiol Soc. 1999;41(6):1147.

70. Firmin DN, Nayler GL, Kilner PJ, Longmore DB. The application of phase shifts in NMR for flow measurement. Magn Reson Med. 1990;14(2):230–41.

71. Buss SJ, Krautz B, Schnackenburg B, Abdel-Aty H, Santos MFB, Andre F, et al. Classification of diastolic function with phase-contrast cardiac magnetic resonance imaging: validation with echocardiography and age-related reference values. Clin Res Cardiol. 2014 Jun;103(6):441–50.

72. Bollache E, Redheuil A, Clément-Guinaudeau S, Defrance C, Perdrix L, Ladouceur M, et al. Automated left ventricular diastolic function evaluation from phase-contrast cardiovascular magnetic resonance and comparison with Doppler echocardiography. J Cardiovasc Magn Reson. 2010;12:63.

73. Speiser U, Quick S, Haas D, Youssef A, Waessnig NK, Ibrahim K, et al. 3-T magnetic resonance for determination of aortic valve area: A comparison to echocardiography. Scand Cardiovasc J. 2014 Jun;48(3):176–83.

74. Defrance C, Bollache E, Kachenoura N, Perdrix L, Hrynchyshyn N, Bruguiere E, et al. Evaluation of Aortic Valve Stenosis Using Cardiovascular Magnetic Resonance: Comparison of an Original Semiautomated Analysis of Phase-Contrast Cardiovascular Magnetic Resonance With Doppler Echocardiography. Circ Cardiovasc Imaging. 2012 Sep 1;5(5):604–12.

75. Mostbeck GH, Hartiala JJ, Foster E, Fujita N, Dulce MC, Higgins CB. Right ventricular diastolic filling: evaluation with velocity-encoded cine MRI. J Comput Assist Tomogr. 1993 Apr;17(2):245–52.

76. Bland JM, Altman D. Statistical methods for assessing agreement between two methods of clinical measurement. The lancet. 1986;327(8476):307–10.

77. Koo TK, Li MY. A Guideline of Selecting and Reporting Intraclass Correlation Coefficients for Reliability Research. J Chiropr Med. 2016 Jun;15(2):155–63.

78. Stojanov D, Aracki-Trenkic A, Benedeto-Stojanov D. Gadolinium deposition within the dentate nucleus and globus pallidus after repeated administrations of gadolinium-based contrast agents-current status. Neuroradiology. 2016 May;58(5):433–41.

79. Dillman JR, Davenport MS. Gadolinium retention — 5 years later…. Pediatr Radiol. 2020 Feb 1;50(2):166–7.

80. McDonald RJ, McDonald JS, Kallmes DF, Jentoft ME, Murray DL, Thielen KR, et al. Intracranial Gadolinium Deposition after Contrast-enhanced MR Imaging. Radiology. 2015 Jun;275(3):772–82.

81. Bussi S, Penard L, Bonafè R, Botteron C, Celeste R, Coppo A, et al. Non-clinical assessment of safety and gadolinium deposition after cumulative administration of gadobenate dimeglumine (MultiHance®) to neonatal and juvenile rats. Regul Toxicol Pharmacol RTP. 2018 Feb;92:268–77.

82. Kanda T, Osawa M, Oba H, Toyoda K, Kotoku J, Haruyama T, et al. High Signal Intensity in Dentate Nucleus on Unenhanced T1-weighted MR Images: Association with Linear versus Macrocyclic Gadolinium Chelate Administration. Radiology. 2015 Jun;275(3):803–9.

83. Radbruch A, Weberling LD, Kieslich PJ, Hepp J, Kickingereder P, Wick W, et al. Intraindividual Analysis of Signal Intensity Changes in the Dentate Nucleus After Consecutive Serial Applications of Linear and Macrocyclic Gadolinium-Based Contrast Agents. Invest Radiol. 2016 Nov;51(11):683.

84. Cao Y, Huang DQ, Shih G, Prince MR. Signal Change in the Dentate Nucleus on T1-Weighted MR Images After Multiple Administrations of Gadopentetate Dimeglumine Versus Gadobutrol. Am J Roentgenol. 2016 Feb;206(2):414–9.

85. Radbruch A, Weberling LD, Kieslich PJ, Eidel O, Burth S, Kickingereder P, et al. Gadolinium Retention in the Dentate Nucleus and Globus Pallidus Is Dependent on the Class of Contrast Agent. Radiology. 2015 Jun;275(3):783–91.

86. Radbruch A, Weberling LD, Kieslich PJ, Hepp J, Kickingereder P, Wick W, et al. High-Signal Intensity in the Dentate Nucleus and Globus Pallidus on Unenhanced T1-Weighted Images: Evaluation of the Macrocyclic Gadolinium-Based Contrast Agent Gadobutrol. Invest Radiol. 2015 Dec;50(12):805.

87. Welk B, McArthur E, Morrow SA, MacDonald P, Hayward J, Leung A, et al. Association Between Gadolinium Contrast Exposure and the Risk of Parkinsonism. JAMA. 2016 Jul 5;316(1):96–8.

88. Perrotta G, Metens T, Absil J, Lemort M, Manto M. Absence of clinical cerebellar syndrome after serial injections of more than 20 doses of

gadoterate, a macrocyclic GBCA: a monocenter retrospective study. J Neurol. 2017 Nov;264(11):2277–83.

89. McDonald RJ, McDonald JS, Kallmes DF, Jentoft ME, Paolini MA, Murray DL, et al. Gadolinium Deposition in Human Brain Tissues after Contrast-enhanced MR Imaging in Adult Patients without Intracranial Abnormalities. Radiology. 2017 Nov;285(2):546–54.

90. McDonald RJ, Levine D, Weinreb J, Kanal E, Davenport MS, Ellis JH, et al. Gadolinium Retention: A Research Roadmap from the 2018 NIH/ACR/RSNA Workshop on Gadolinium Chelates. Radiology. 2018 Nov;289(2):517–34.

91. Gulani V, Calamante F, Shellock FG, Kanal E, Reeder SB. Gadolinium deposition in the brain: summary of evidence and recommendations. Lancet Neurol. 2017 Jul 1;16(7):564–70.

92. Malayeri AA, Brooks KM, Bryant LH, Evers R, Kumar P, Reich DS, et al. National Institutes of Health Perspective on Reports of Gadolinium Deposition in the Brain. J Am Coll Radiol JACR. 2016 Mar;13(3):237–41.

93. Messroghli DR, Radjenovic A, Kozerke S, Higgins DM, Sivananthan MU, Ridgway JP. Modified Look-Locker inversion recovery (MOLLI) for high-resolution T1 mapping of the heart. Magn Reson Med. 2004 Jul 1;52(1):141–6.

94. Rohrer M, Bauer H, Mintorovitch J, Requardt M, Weinmann HJ. Comparison of magnetic properties of MRI contrast media solutions at different magnetic field strengths. Invest Radiol. 2005;40(11):715–24.

95. Lin HY, Bender JA, Ding Y, Chung YC, Hinton AM, Pennell ML, et al. Shared velocity encoding: a method to improve the temporal resolution of phase-contrast velocity measurements. Magn Reson Med. 2012 Sep;68(3):703–10.

96. Lustig M, Donoho D, Pauly JM. Sparse MRI: The application of compressed sensing for rapid MR imaging. Magn Reson Med. 2007;58(6):1182–95.

97. Nickander J, Lundin M, Abdula G, Jenner J, Maret E, Sörensson P, et al. Stationary tissue background correction increases the precision of clinical evaluation of intra-cardiac shunts by cardiovascular magnetic resonance. Sci Rep. 2020 Dec;10(1):5053.

98. Heiberg E, Sjögren J, Ugander M, Carlsson M, Engblom H, Arheden H. Design and validation of Segment--freely available software for cardiovascular image analysis. BMC Med Imaging. 2010;10:1.

99. Klein AL, Abbara S, Agler DA, Appleton CP, Asher CR, Hoit B, et al. American Society of Echocardiography Clinical Recommendations for Multimodality Cardiovascular Imaging of Patients with Pericardial Disease. J Am Soc Echocardiogr. 2013 Sep;26(9):965-1012.e15.

100. Bland JM, Altman DG. Measuring agreement in method comparison studies. Stat Methods Med Res. 1999 Jun;8(2):135–60.

101. Ben-Horin S, Bank I, Shinfeld A, Kachel E, Guetta V, Livneh A. Diagnostic value of the biochemical composition of pericardial effusions in patients undergoing pericardiocentesis. Am J Cardiol. 2007 May 1;99(9):1294–7.

102. Frola C, Cantoni S, Turtulici I, Leoni C, Loria F, Gaeta M, et al. Transudative vs exudative pleural effusions: differentiation using Gd-DTPA-enhanced MRI. Eur Radiol. 1997;7(6):860–4.

103. Ugander M, Oki AJ, Hsu LY, Kellman P, Greiser A, Aletras AH, et al. Extracellular volume imaging by magnetic resonance imaging provides insights into overt and sub-clinical myocardial pathology. Eur Heart J. 2012 May 2;33(10):1268–78.

104. Nandalur KR, Hardie AH, Bollampally SR, Parmar JP, Hagspiel KD. Accuracy of Computed Tomography Attenuation Values in the Characterization of Pleural Fluid. Acad Radiol. 2005 Aug;12(8):987–91.

105. Çullu N, Kalemci S, Karakaş Ö, Eser İ, Yalçin F, Boyacı FN, et al. Efficacy of CT in diagnosis of transudates and exudates in patients with pleural effusion. Diagn Interv Radiol Ank Turk. 2014 Apr;20(2):116–20.

106. Tomoda H, Hoshiai M, Furuya H, Oeda Y, Matsumoto S, Tanabe T, et al. Evaluation of pericardial effusion with computed tomography. Am Heart J. 1980 Jun;99(6):701–6.

107. Abramowitz Y, Simanovsky N, Goldstein MS, Hiller N. Pleural Effusion: Characterization with CT Attenuation Values and CT Appearance. Am J Roentgenol. 2009 Mar;192(3):618–23.

108. Avery LL, Jain VR, Cohen HW, Scheinfeld MH. High attenuation pericardial fluid on CT following cardiac catheterization. Emerg Radiol. 2014;21(4):381–6.

109. Çetin MS, Özcan Çetin EH, Özdemir M, Topaloğlu S, Aras D, Temizhan A, et al. Effectiveness of computed tomography attenuation values in characterization of pericardial effusion. Anatol J Cardiol. 2017 Apr;17(4):322–7.

110. Bourin M, Jolliet P, Ballereau F. An overview of the clinical pharmacokinetics of x-ray contrast media. Clin Pharmacokinet. 1997;32(3):180–93.

111. Bellin MF, Van Der Molen AJ. Extracellular gadolinium-based contrast media: An overview. Eur J Radiol. 2008 May;66(2):160–7.

112. Nacif MS, Kawel N, Lee JJ, Chen X, Yao J, Zavodni A, et al. Interstitial myocardial fibrosis assessed as extracellular volume fraction with low-radiation-dose cardiac CT. Radiology. 2012;264(3):876–83.

113. Adler Y, Charron P, Imazio M, Badano L, Barón-Esquivias G, Bogaert J, et al. 2015 ESC Guidelines for the diagnosis and management of pericardial diseases. Eur Heart J. 2015 Nov 7;36(42):2921–64.

114. Rosmini S, Seraphim A, Knott K, Brown JT, Knight DS, Zaman S, et al. Non-invasive characterization of pleural and pericardial effusions using T1 mapping by magnetic resonance imaging. Eur Heart J Cardiovasc Imaging. 2021 Jul 30;jeab128.

115. Ben-Horin S, Shinfeld A, Kachel E, Chetrit A, Livneh A. The composition of normal pericardial fluid and its implications for diagnosing pericardial effusions. Am J Med. 2005 Jun;118(6):636–40.

116. Kuetting D, Luetkens J, Faron A, Isaak A, Attenberger U, Pieper CC, et al. Evaluation of malignant effusions using MR-based T1 mapping. Sci Rep. 2021 Mar 29;11(1):7116.

117. Kramer CM, Barkhausen J, Bucciarelli-Ducci C, Flamm SD, Kim RJ, Nagel E. Standardized cardiovascular magnetic resonance imaging (CMR) protocols: 2020 update. J Cardiovasc Magn Reson. 2020 Feb 24;22(1):17.

118. Chow K, Flewitt JA, Green JD, Pagano JJ, Friedrich MG, Thompson RB. Saturation recovery single-shot acquisition (SASHA) for myocardial T(1) mapping. Magn Reson Med. 2014 Jun;71(6):2082–95.

119. Piechnik SK, Ferreira VM, Dall'Armellina E, Cochlin LE, Greiser A, Neubauer S, et al. Shortened Modified Look-Locker Inversion recovery (ShMOLLI) for clinical myocardial T1-mapping at 1.5 and 3 T within a 9 heartbeat breathhold. J Cardiovasc Magn Reson. 2010;12(1):69.

120. Weingärtner S, Akcakaya M, Berg S, Kissinger KV, Manning WJ, Nezafat R. Heart-rate independent myocardial T1-mapping using combined saturation and inversion preparation pulses. J Cardiovasc Magn Reson. 2013 Jan 30;15(Suppl 1):P46.

121. Kellman P, Hansen MS. T1-mapping in the heart: accuracy and precision. J Cardiovasc Magn Reson. 2014;16(1):2.

122. Nagueh SF, Smiseth OA, Appleton CP, Byrd BF, Dokainish H, Edvardsen T, et al. Recommendations for the Evaluation of Left Ventricular Diastolic Function by Echocardiography: An Update from the American Society of Echocardiography and the European Association of Cardiovascular Imaging. J Am Soc Echocardiogr. 2016 Apr;29(4):277–314.

123. Ginghina C, Beladan C, Iancu M, Calin A, Popescu BA. Respiratory maneuvers in echocardiography: A review of clinical applications. Vol. 7. 2009. 42 p.

124. Burstow DJ, Oh JK, Bailey KR, Seward JB, Tajik AJ. Cardiac Tamponade: Characteristic Doppler Observations. Mayo Clin Proc. 1989 Mar;64(3):312–24.

125. Zhang S, Kerins DM, Iii BFB. Doppler Echocardiography in Cardiac Tamponade and Constrictive Pericarditis. Echocardiography. 1994;11(5):507–21.

126. Kim JS, Ha JW, Im E, Park S, Choi EY, Cho YH, et al. Effects of pericardiectomy on early diastolic mitral annular velocity in patients with constrictive pericarditis. Int J Cardiol. 2009 Mar 20;133(1):18–22.

127. Appleton C, Gillam L, Koulogiannis K. Cardiac Tamponade. Cardiol Clin. 2017 Nov 1;35(4):525–37.

128. Dornhorst AC, Howard P, Leathart GL. Pulsus paradoxus. Lancet Lond Engl. 1952 Apr 12;1(6711):746–8.

129. Hatle LK, Appleton CP, Popp RL. Differentiation of constrictive pericarditis and restrictive cardiomyopathy by Doppler echocardiography. Circulation. 1989;79(2):357–70.

130. Picard MH, Sanfilippo AJ, Newell JB, Rodriguez L, Guerrero JL, Weyman AE. Quantitative relation between increased intrapericardial pressure and Doppler flow velocities during experimental cardiac tamponade. J Am Coll Cardiol. 1991 Jul;18(1):234–42.

131. Gonzalez MS, Basnight MA, Appleton CP. Experimental pericardial effusion: relation of abnormal respiratory variation in mitral flow velocity to hemodynamics and diastolic right heart collapse. J Am Coll Cardiol. 1991;17(1):239–48.

132. Kovacs SJJ, Barzilai B, Perez JE. Evaluation of diastolic function with Doppler echocardiography: the PDF formalism. Am J Physiol. 1987 Jan;252(1 Pt 2):H178-187.